







## REVIEW

[View Article Online](#)  
[View Journal](#) | [View Issue](#)Cite this: *Chem. Sci.*, 2025, 16, 11711Dual-metal synergistic catalysis for promoting electrocatalytic CO<sub>2</sub> reductionPeng-Yu Shi,  † Yan Yan,  † Si-Yuan Yang,  Jing-Jing Hao,  Mei Wang  \* and Tong-Bu Lu  \*

The increasing emphasis on carbon neutrality has driven significant research into the electrochemical CO<sub>2</sub> reduction reaction (CO<sub>2</sub>RR), aiming to convert CO<sub>2</sub> into value-added chemicals and fuels. Dual-metal catalysts, known for their synergistic effects, have garnered considerable attention due to their enhanced electrocatalytic performance for the CO<sub>2</sub>RR by providing more active sites and optimizing intermediate interactions. Herein, this review will comprehensively explore how the synergistic effect between the two metal centers embedded within atomic and nanoparticle dual-metal catalysts facilitates the electrocatalytic CO<sub>2</sub>RR, elucidating the structure–activity correlations. Recent significant progress of dual-metal catalysts with synergistic effects for promoting electrocatalytic CO<sub>2</sub> reduction will be summarized. Moreover, we will explore the design strategies of dual-metal catalysts and examine the influence of different types of metal active centers in the catalysts on the reaction pathway of the electrocatalytic CO<sub>2</sub>RR, aiming to uncover profound insights for catalyst optimization and deepen mechanistic understanding of the catalytic process. Finally, the review identifies current research gaps and outlines future directions, emphasizing the need for innovative techniques to enhance catalytic stability and achieve multi-carbon products from the CO<sub>2</sub>RR using dual-metal catalysts with synergistic effects. This topic could inspire extensive interest to further accelerate and explore the innovations of catalysts in energy conversion.

Received 1st May 2025  
Accepted 4th June 2025

DOI: 10.1039/d5sc03193a

[rsc.li/chemical-science](https://rsc.li/chemical-science)

## 1 Introduction

The combustion of fossil fuels leads to substantial emissions of carbon dioxide and other greenhouse gases, exacerbating global warming and posing a grave threat to human survival and sustainable development.<sup>1–6</sup> Consequently, achieving carbon neutrality and mitigating temperature rise has garnered global consensus.<sup>7–11</sup> The conversion of CO<sub>2</sub> into high-value-added chemicals and fuels offers a promising pathway to close the artificial carbon cycle and address the environmental challenges caused by excessive CO<sub>2</sub> emissions.<sup>12–16</sup>

In CO<sub>2</sub>, the carbon atom forms two strong C=O double bonds, each comprising a sigma ( $\sigma$ ) and a pi ( $\pi$ ) bond, ensuring its high chemical stability. This results in significant thermodynamic and kinetic barriers for the activation of CO<sub>2</sub>, making its conversion pathways both critical and challenging.<sup>17–20</sup> Hence, developing effective methodologies and efficient catalysts holds great significance in advancing the carbon dioxide reduction reaction (CO<sub>2</sub>RR). Various chemical methods have been utilized for CO<sub>2</sub> reduction, including electrocatalysis,

thermal catalysis, photocatalysis, and bioconversion.<sup>21–26</sup> Electrocatalytic (CO<sub>2</sub>RR) technology offers advantages such as simple equipment requirements, high environmental compatibility, and potential integration with intermittent or renewable electricity sources, making it a promising strategy for efficient CO<sub>2</sub> conversion.<sup>27–29</sup>

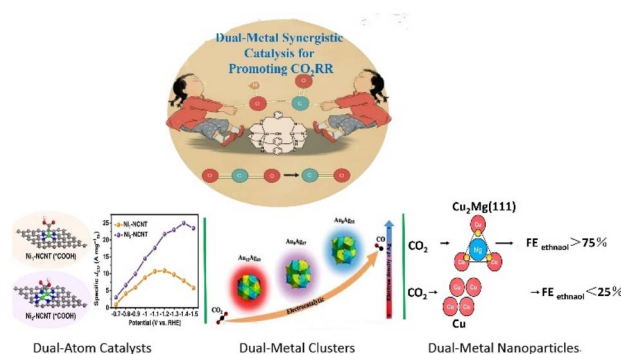
To date, significant advancements have been made in the field of the electrocatalytic CO<sub>2</sub>RR. Various catalyst systems, ranging from nanomaterial catalysts to atomic catalysts, have been meticulously developed to tackle this complex process.<sup>30–34</sup> However, the intricacies of the multi-electron and multi-proton transfer reactions involved in the CO<sub>2</sub>RR have posed numerous challenges, such as low efficiency, sluggish reaction rates and insufficient stability.<sup>35–37</sup> Among all types of catalysts, dual-metal catalysts have garnered particular attention. The modulation of CO<sub>2</sub>RR catalysts with different active sites plays a vital role in solving the existing critical issues.<sup>38</sup> By introducing dual metal active sites into the catalysts, the electronic and geometric properties of the catalysts can be manipulated.<sup>1,9,37,39</sup> Crucially, this approach enables the realization of synergistic catalytic effects. For instance, such synergistic effects can be achieved wherein one metal site facilitates CO<sub>2</sub> activation while another one provides H<sup>+</sup> ions for CO<sub>2</sub> protonation.<sup>40</sup> Thereby, the synergistic effects between different active centres can lead to the optimization of the adsorption and activation of

School of Materials Science and Engineering, Institute for New Energy Materials & Low Carbon Technologies, Tianjin University of Technology, Tianjin 300384, China.  
E-mail: [meiwan@email.tjut.edu.cn](mailto:meiwan@email.tjut.edu.cn); [lutongbu@tjut.edu.cn](mailto:lutongbu@tjut.edu.cn)

† These authors contributed equally to this work.

reactants, transition state stabilization, and the desorption of products, as well as the refinement of the catalytic pathway for optimal performance for CO<sub>2</sub> reduction. The dual-metal catalysts can be broadly classified into two types: dual-atom metal catalysts and dual-metal nanomaterial catalysts.<sup>1,9,41,42</sup> Dual-atom catalysts can further be subdivided into homonuclear and heteronuclear dual-atom catalysts. Compared to single-atom catalysts, dual-atom catalysts offer much more advantages such as higher metal loading, more active sites, and more flexible adjustability for the CO<sub>2</sub>RR.<sup>43,44</sup> By tuning the composition and arrangement of the two metal atoms in dual-atom catalysts, enhanced catalytic efficiency can be achieved compared to single-atom catalysts for the CO<sub>2</sub>RR.<sup>45,46</sup> The synergistic effect between the two metal atoms can decrease the activation barriers for CO<sub>2</sub>, directing the reaction pathway towards high selectivity. For example, Lu *et al.* reported an asymmetric TeN<sub>2</sub>-CuN<sub>3</sub> catalyst with a synergistic mechanism: Te activates CO<sub>2</sub>, while Cu aids H<sub>2</sub>O dissociation, which significantly reduces the energy barrier and improves proton transfer kinetics for CO<sub>2</sub>-to-CO reduction.<sup>40</sup> Dual-metal nanomaterial catalysts constitute another crucial class of catalysts for the electrochemical CO<sub>2</sub>RR, experiencing notable advancements.<sup>31</sup> The copper metal exhibits weak hydrogen adsorption but moderate CO adsorption, effectively suppressing the hydrogen evolution (HER) and uniquely facilitating efficient production of multi-carbon products in CO<sub>2</sub> electroreduction.<sup>47</sup> Therefore, copper-based dual-metal nanomaterial catalysts stand out due to their distinct advantages in the electrocatalytic CO<sub>2</sub>RR, demonstrating remarkable potential in facilitating the production of high-value C<sub>2+</sub> products. For instance, Wang *et al.* constructed Ag-Cu dual sites in Ag-doped Cu<sub>3</sub>N NC (Cu<sub>3</sub>N-Ag NC), where CO is produced on Ag sites, and asymmetric C-C coupling to COCHO is promoted on Cu sites, leading to a marked increase in Faraday efficiency (FE) for C<sub>2</sub>H<sub>4</sub> production compared to that of pure Cu<sub>3</sub>N NC, which highlights the crucial role of the synergistic effects between the dual-metal Ag and Cu in the formation of multicarbon products.<sup>48</sup> There have been many reviews on electrocatalytic CO<sub>2</sub> reduction. Nevertheless, to date, there has been no review devoted to the impact of the synergistic effect of dual-active sites in the catalysts on the reaction pathway for the CO<sub>2</sub>RR, which is of great significance in this area.

In this review, our primary goal is to offer a thorough examination of how dual-metal systems leverage their synergistic effects to optimize both electronic and geometric structures. Concurrently, these optimizations serve to enhance the functionality of dual-active sites, thereby achieving superior electrocatalytic performance towards the CO<sub>2</sub>RR. First, we will delve into uncovering the design principles underlying dual-metal systems for the CO<sub>2</sub>RR, with a primary focus on two key aspects: the precise modulation of the electronic structure and the control of the geometric configuration. In terms of electronic structure regulation, we will scrutinize three primary approaches such as chemical state, vacancy, and coordination environment modifications. Regarding geometric structure control, we will focus on several key parameters such as crystal facet, nanoparticle size, and morphology adjustments.



**Scheme 1** Different types of dual-metal catalysts with synergistic effects for promoting electrocatalytic CO<sub>2</sub> reduction. Reproduced with permission.<sup>124</sup> Copyright 2023, Elsevier. Reproduced with permission.<sup>96</sup> Copyright 2023, Wiley-VCH Verlag. Reproduced with permission.<sup>99</sup> Copyright 2024, John Wiley and Sons Ltd.

Furthermore, we will systematically probe the way varying dual-metal active sites embedded within atomic (notably dual-atom catalysts, DACs) and nanoparticle catalysts affect CO<sub>2</sub>RR catalytic performance, elucidating the pivotal role of synergistic effects in the fundamental reaction mechanisms. Specifically, we will investigate the synergistic dynamics within homonuclear and heteronuclear DACs systems. Additionally, an in-depth analysis will be conducted on nanomaterial catalysts that pair copper with main-group elements, non-precious metals, precious metals, and lanthanides, to elucidate their effects on catalytic mechanisms and overall efficiency in the CO<sub>2</sub>RR. Finally, we identify the prevalent challenges and promising directions for the ongoing advancement of dual-metal catalysts, with the goal of enhancing electrocatalytic efficiency and stability for the production of multi-carbon compounds through the CO<sub>2</sub>RR. This review will provide profound and insightful perspectives, thereby facilitating the rapid acceleration and in-depth exploration of innovations in dual-metal catalysts within the domain of energy conversion (Scheme 1).

## 2 Design principles of dual-metal catalysts with synergistic effects for the electrocatalytic CO<sub>2</sub>RR

A vast array of design approaches has been meticulously investigated to enhance the electrocatalytic performance for the CO<sub>2</sub>RR. The key design principles for dual-metal catalysts in the electrocatalytic CO<sub>2</sub>RR involve electronic and geometric aspects, as these factors critically govern the formation of key intermediates, the pathway of C-C coupling, and the ability to suppress hydrogen evolution.<sup>49</sup> The electronic structure dictates the intrinsic catalytic properties by modulating the binding energy of reaction intermediates and steering the reaction pathway, while the geometric structure controls the physical arrangement of active sites, influencing reactant accessibility, mass transport, and the exposure of specific catalytic facets. By optimizing both of these aspects, dual-metal catalysts can



achieve enhanced efficiency and selectivity for converting CO<sub>2</sub> into valuable products. Therefore, prioritizing electronic and geometric structure regulation is essential for designing advanced catalysts that maximize performance and contribute to sustainable CO<sub>2</sub> utilization.<sup>50</sup>

## 2.1 Electronic structure regulation

Electronic structure regulation is a critical aspect of dual-metal catalyst design. By adjusting the chemical state of the metals, the valence state of the active sites can be stabilized or altered, which in turn influences their catalytic activity for the electrocatalytic CO<sub>2</sub>RR.<sup>51</sup> Additionally, the incorporation of dual-metal catalysts can lead to the formation of vacancies or defects within the catalyst structure, which can highly tune the electronic structure of the catalyst.<sup>52,53</sup> Furthermore, coordination environment regulation can alter the local electronic sphere of metal active sites with synergistic interactions between the two metals, enhancing catalytic performance by tuning the energy levels of key intermediates during the CO<sub>2</sub>RR process.<sup>54</sup>

**2.1.1 Chemical state regulation.** The valence state of the active sites is the most critical factor determining the catalytic efficiency of the catalyst for the electrocatalytic CO<sub>2</sub>RR. By precisely regulating the chemical states, the reaction way can be steered towards the production of desired compounds, while minimizing the formation of byproducts, which is crucial for enhancing the efficiency of the CO<sub>2</sub>RR.<sup>55,56</sup> For instance, previous studies have demonstrated that the Cu<sup>+</sup>/Cu<sup>0</sup> mixed state plays a critical role in CO<sub>2</sub> electroreduction to multi-carbon (C<sub>2+</sub>) *via* reducing the kinetic barrier to C–C coupling.<sup>57</sup>

Dual-metal catalysts can leverage the tight interactions between two distinct metals to stabilize and/or modulate the chemical state of active sites. The electron density around the active sites can be modulated by the synergistic interaction between the two metals. Fine-tuning the valence states in dual-metal catalysts can lead to optimal adsorption and activation of CO<sub>2</sub> molecules, as well as the stabilization of key intermediates, thereby influencing its catalytic activity and product efficiency for the electrocatalytic CO<sub>2</sub>RR.<sup>58</sup>

Many non-noble transition metals, such as Fe, Co, Ni, and Zn are used to as the second metal to stabilize the oxidation state of active metal sites, leveraging the synergistic catalytic effect of the two metals to enhance the performance of the electrocatalytic CO<sub>2</sub>RR.<sup>59–61</sup> For example, Ma and Zhang's group reported that incorporating Ni into CuO nanosheets can stabilize the chemical state of Cu, meanwhile reinforcing the connections between Cu atoms located on the surface and those beneath the surface, resulting in a sustained FE<sub>C<sub>2+</sub></sub> and improved stability for the electrocatalytic CO<sub>2</sub>RR compared to pure CuO nanosheets (Fig. 1a).<sup>62</sup> Choi *et al.* demonstrated that incorporating Zn into Cu<sub>2</sub>O achieves two significant effects: it can stabilize Cu in a lower valence state (Cu<sup>0</sup>), which is more active for CO<sub>2</sub> reduction; and it can lower the energy barrier for the OHC–CHO C–C coupling pathway, thereby promoting the formation of C<sub>2</sub>H<sub>4</sub>. These beneficial effects can be attributed to the charge transfer from Zn to Cu, which reduces Cu<sup>+</sup> to a lower and stable valence state and facilitates a more favorable

reduction reaction at the Cu site (Fig. 1b).<sup>56</sup> Therefore, the combination of a second metal with the copper based catalyst can stabilize the valence state of the active site, leading to improve catalytic performance for the CO<sub>2</sub>RR due to the synergistic effect.

In addition to maintaining the constant chemical state of the active sites, the second metal can also effectively regulate the chemical state of the active metal centers. Many noble metals or main group metals are used to modulate the oxidation state of the metal active centers. Kim *et al.* underscored the pivotal role of modulating the oxidation state by decorating copper (Cu) nanoparticles with iridium (Ir), leading to the charge transfer from Cu to Ir, which indicates that the oxidation state of Cu in the CuIr alloy is higher than that in Cu nanoparticles. By exploiting the robust affinity of Ir for oxygen, the electronic configuration of Cu is effectively modulated, thereby stabilizing oxygen-bound intermediates like CH<sub>3</sub>CHO\* and CH<sub>3</sub>CH<sub>2</sub>O\* during the CO<sub>2</sub>RR that are otherwise unstable on bare Cu catalysts. This valence state adjustment strategy markedly boosted the FE to 14.8% for reducing CO<sub>2</sub> to *tert*-butanol (*t*-BuOH), which represents a substantial improvement compared to that of pure Cu catalysts (Fig. 1c).<sup>63</sup> Loh's group constructed a Cu/CaCO<sub>3</sub> catalyst for the CO<sub>2</sub>RR by integrating Cu nano-clusters with CaCO<sub>3</sub>, in which the metal Ca can regulate the formation of dynamically stable Cu<sup>0</sup>/Cu<sup>δ+</sup> pair sites and maintain the Cu<sup>δ+</sup> valence state. Consequently, the synergistic effect of the dual metal Cu and Ca can enhance adsorption capacity of CO<sub>2</sub> intermediate \*CO and lower the C–C coupling energy barriers, achieving a remarkable FE of 83.7% for C<sub>2+</sub> at a partial current density of 393 mA cm<sup>−2</sup> (Fig. 1d).<sup>64</sup> The strategy of introducing a second metal to stabilize or modulate the valence state of catalytic centers is of great significance in designing and synthesizing highly efficient dual-metal catalysts. This approach can optimize intermediate binding, lower energy barriers and significantly enhance the electrocatalytic performance for the CO<sub>2</sub>RR.

**2.1.2 Vacancy regulation.** Considerable progress has been made in developing dual-metal catalysts with enhanced efficiency through vacancy engineering, aimed at converting CO<sub>2</sub> into valuable chemicals. The vacancies within dual-metal catalysts have the ability to tune the electronic structure of the catalyst. The presence of vacancies can regulate the electronic cloud distribution around the metal atoms, and also create localized regions of high electron density leading to changes in energy levels and bonding properties. Specifically, these electron-rich sites are particularly well-suited for interacting with CO<sub>2</sub>. Meanwhile, by serving as electron donors, the vacancy sites aid in weakening the double bonds in CO<sub>2</sub> and facilitate the formation of intermediate species, enhancing the overall electrocatalytic CO<sub>2</sub>RR process.<sup>65</sup>

Of particular note are cationic vacancies, which have unique electronic structures and orbital distributions, and can greatly affect the properties of the metal catalysts for CO<sub>2</sub> reduction.<sup>66–70</sup> For instance, Sun *et al.* reported that introducing Sn dopants into a copper catalyst could modify the lattice structure of CuO, giving rise to the formation of oxygen vacancies, which have a significant impact on the surface electron distribution of the





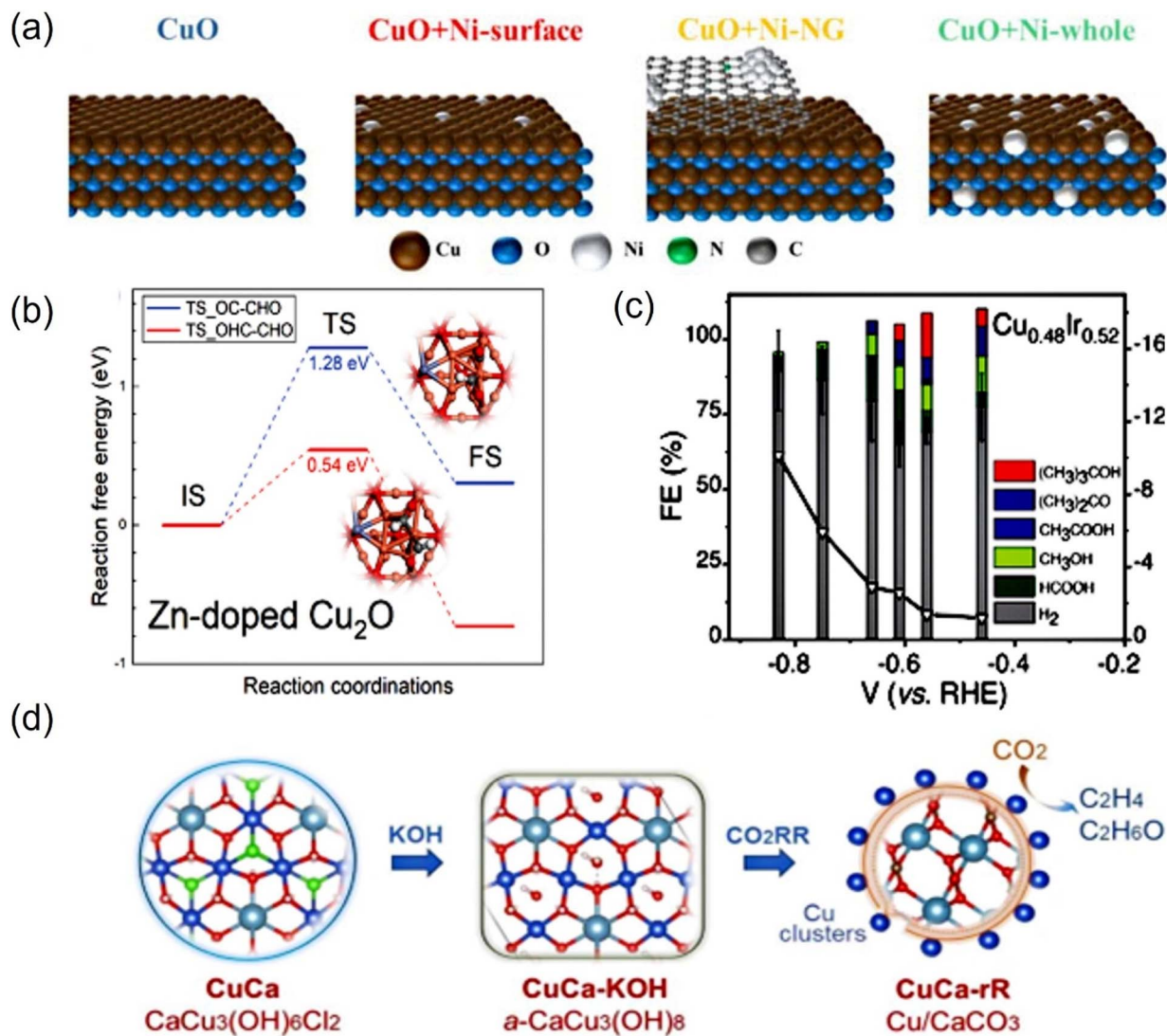


Fig. 1 (a) Different Ni-incorporated Cu catalysts. (b) Activation barrier diagram of C–C coupling on Zn-doped Cu<sub>2</sub>O. (c) Potential-dependent faradaic efficiencies (FEs) for CO<sub>2</sub>RR products and total current densities obtained by using Cu<sub>0.48</sub>Ir<sub>0.52</sub>. (d) Scheme of the reconstruction process to obtain Cu/CaCO<sub>3</sub>. (a) Reproduced with permission.<sup>62</sup> Copyright 2025, Elsevier. (b) Reproduced with permission.<sup>56</sup> Copyright 2023, Wiley. (c) Reproduced with permission.<sup>63</sup> Copyright, 2023, Wiley. (d) Reproduced with permission.<sup>64</sup> Copyright 2025, John Wiley and Sons Ltd.

CuO nanosheets. DFT calculations confirmed that the synergistic effect of oxygen vacancies and the metals can strengthen CO<sub>2</sub> adsorption and reduce the energy barrier for the formation of intermediate species such as \*COOH and \*CO during the electroreduction process, leading to a substantial enhancement in the efficiency for electrocatalytic CO<sub>2</sub> reduction to CO (Fig. 2a).<sup>71</sup> Similarly, He, Xu, *et al.* constructed a series of dual-metal Cu/Ce catalysts with different concentrations of oxygen vacancies, in which the oxygen vacancies could alter the electronic microenvironment of the catalyst, leading to the introduction of uncoordinated metal site Cu<sup>+</sup> active centers. This revealed that the high concentration of oxygen vacancies in the dual-metal catalyst is crucial for facilitating the adsorption of \*COOH and \*CO intermediates, resulting in the efficient production of CH<sub>4</sub> with a FE of 70.03% and a TOF of 9946.7 h<sup>-1</sup> (Fig. 2b).<sup>70</sup>

In addition to tuning the electronic structure of the catalyst, these vacancies in dual-metal catalysts can also act as active sites for the adsorption and conversion of CO<sub>2</sub>. Xiao *et al.* doped Cu into ZnO, inducing a synergistic effect that generated abundant oxygen vacancies. These vacancies can not only modulate the local electronic structure of the active sites but also serve as electron-trapping centers, facilitating CO<sub>2</sub> adsorption and promoting electron transfer for its reduction. Additionally, they could also suppress the HER, thereby lowering the energy barrier for electrocatalytic CO<sub>2</sub> conversion to CO, leading to a high FE<sub>CO</sub> > 80% within a wide potential range.<sup>72</sup> In dual-metal catalysts, the cooperation between the two metals may also lead to the formation of vacancies within certain metal cations. These vacancies, akin to those in anion sites, possess the ability to regulate the electronic structure and also serve as catalytic centers, thereby influencing the adsorption and activation of

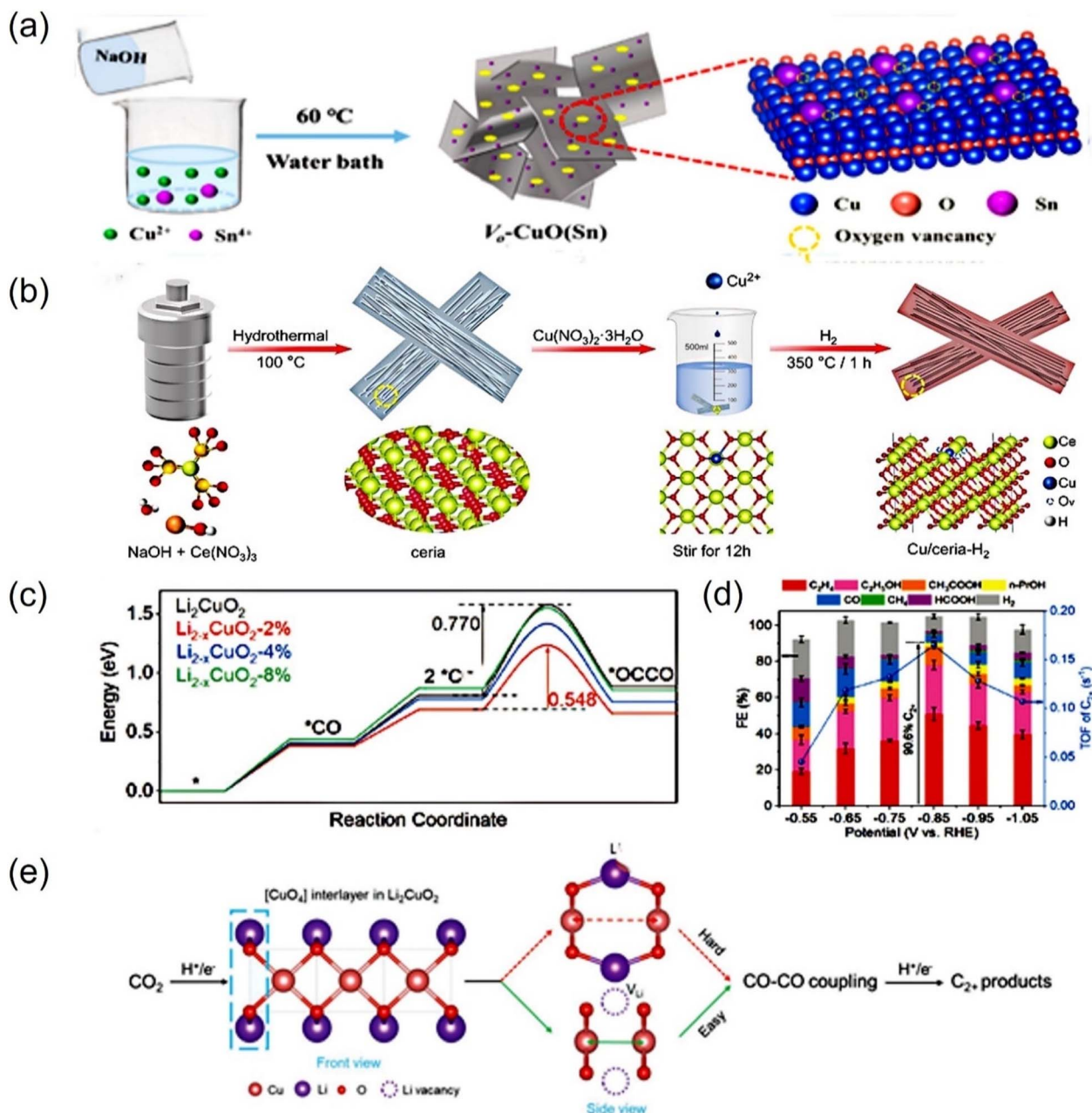


Fig. 2 (a) Schematic illustration of the synthesis of  $\text{Vo-CuO(Sn)}$ . (b) Schematic illustration for the synthesis of the  $\text{Cu/ceria-H}_2$  catalyst. (c) Corresponding energy diagrams of C-C coupling for pristine  $\text{Li}_2\text{CuO}_2$ ,  $\text{Li}_{2-x}\text{CuO}_2$ -2%,  $\text{Li}_{2-x}\text{CuO}_2$ -4%, and  $\text{Li}_{2-x}\text{CuO}_2$ -8%. (d) Faradaic efficiencies for  $\text{CO}_2\text{RR}$  products and TOF values for  $\text{C}_{2+}$  products on the  $\text{Li}_{2-x}\text{CuO}_2$  catalyst. (e) Scheme of  $\text{Li}^+$  vacancy-tuned  $[\text{CuO}_4]$  sites that promote C-C coupling. (a) Reproduced with permission.<sup>71</sup> Copyright 2022, American Chemical Society. (b) Reproduced with permission.<sup>70</sup> Copyright 2025, John Wiley and Sons Ltd. (c-e) Reproduced with permission.<sup>73</sup> Copyright 2022, Wiley-VCH Verlag.

$\text{CO}_2$ . Zheng, Li, *et al.* incorporated the second metal lithium (Li) into the copper oxides to construct the dual-metal catalyst  $\text{Li}_2\text{CuO}_2$ , constructing  $\text{Li}^+$  vacancies, which can tailor the electronic structure and regulate the adsorption energies of intermediate species. It can lower the coordination number of  $\text{Li}^+$  around each Cu atom, which highly facilitated the  $\text{CO-CO}$  coupling, while impeding the competitive HER through suppressing the adsorption of  $\text{*H}$  intermediates, resulting in the highest FE of 90.6% for  $\text{C}_{2+}$  products (Fig. 2c-e).<sup>73</sup>

The design and synthesis of dual-metal catalysts containing vacancies with synergistic catalytic effects offer distinct advantages in optimizing the electronic structure of the catalyst and enhancing catalytic efficiency for the  $\text{CO}_2\text{RR}$ . These vacancies not only improve the interaction with reactants but also serve as active sites for catalyzing the  $\text{CO}_2\text{RR}$ . Precise control over the vacancy position, quantity, and type can thus optimize the dual-metal catalyst's electronic structure and performance, offering a novel strategy for efficient  $\text{CO}_2$  conversion.

**2.1.3 Coordination environment regulation.** The regulation of metal coordination environments involves several key aspects, such as the types of central metal sites, the coordination geometry, the coordination number, the type and number of the coordinating atoms, and the first and second coordination shell, each of which can significantly influence the properties and functionalities of dual-metal systems for CO<sub>2</sub> conversion.<sup>74</sup> It is noteworthy that the synergistic interaction between two metals can also modulate the coordination environment of the active metal center, fine-tuning its electronic structure.<sup>33,75</sup> Meanwhile, the regulation of the coordination environment can further enhance the synergistic catalytic effect between metals in dual-metal catalysts, thereby improving the catalyst's ability for the electrocatalytic CO<sub>2</sub>RR. Such a modulation not only elucidates the mechanisms of metal interactions but also provides a theoretical basis for designing high-performance catalysts.<sup>76</sup>

Ligands with varying electronegativities such as N, O, S, and P can alter the electron density of metal active centers. For example, electron-withdrawing ligands can lower the energy of metal d-orbitals, weakening intermediate adsorption, while electron-donating ligands can enhance adsorption and promote CO<sub>2</sub> activation.<sup>38,77–79</sup> Voiry *et al.* introduced electron-withdrawing ligand groups such as N<sub>2</sub>SN–, N<sub>3</sub>N– and C<sub>2</sub>N– to tailor the surface coordination environment of a dual-metal Cu–Ag electrocatalyst for CO<sub>2</sub> reduction. Notably, the ligands N<sub>2</sub>SN– and N<sub>3</sub>N– were found to stabilize the Cu center in a low oxidation state ( $0 < \delta < +1$ ), which critically modulated the electronic structure of the dual-metal Ag–Cu catalyst. This ligand-induced electronic perturbation enhanced the synergistic cooperation between Ag and Cu, promoting CO<sub>2</sub> adsorption and regulating the reduction pathways. Consequently, the optimized catalyst achieved efficient electrocatalytic conversion of CO<sub>2</sub> into high-value multicarbon products (Fig. 3a and b).<sup>80</sup> Zhang *et al.* constructed a redox-active cobalt (Co) protoporphyrin-modified MIL-101(Cr)–NH<sub>2</sub> material for efficient CO<sub>2</sub> electroreduction. The electron-donating ligand –NH<sub>2</sub> group on the coordinated sphere can not only link the Co and Cr sites, increasing the active sites and tuning their electronic structures, but also improve the CO<sub>2</sub> absorption ability, highly optimizing the intermediate \*CO binding energy, leading to high CO<sub>2</sub>-to-CO conversion (Fig. 3c).<sup>81</sup>

Bridging coordination ligands like N, O, S or halogens can enable electron transfer between the dual metals, creating electron transmission channels, leading to a modified electronic structure and superior catalytic performance for CO<sub>2</sub> reduction.<sup>38</sup> For instance, Zn–N<sub>4</sub>-coordinated Cu single atoms in tandem catalysts can facilitate electron flow from Zn to Cu, enhancing CO<sub>2</sub> activation.<sup>82</sup> In another study, Sakamoto, Sekizawa *et al.* developed a robust Br-bridged dinuclear Cu(I) complex, which can efficiently catalyze CO<sub>2</sub> reduction to produce C<sub>3</sub>H<sub>7</sub>OH with high selectivity. The Br bridge can not only modulate the electronic configurations of the dual Cu active sites by stabilizing their low-spin states, but also strengthen the synergistic collaboration between the bridged Cu centers. This dual modulation mechanism effectively

promoted C–C coupling reactions, leading to significantly enhanced C<sub>2+</sub> hydrocarbon productivity.<sup>83</sup> Chen, Zhang, and colleagues developed a dual-atom catalyst featuring sulfur-bridged Cu–S–Ni motifs. The S-bridge architecture could modulate the electronic charge distribution across the Cu and Ni dual-atom centers, while enhancing synergistic effects between the dual-metal sites. This atomic-level cooperation facilitates the critical COOH\* intermediate formation during CO<sub>2</sub> electroreduction, resulting in a remarkable FE of 98.1% for CO production at –0.65 V in a H-cell (Fig. 3d and e).<sup>84</sup>

The synergistic interaction between dual metals, mediated by tailored coordination environments, is critical for optimizing electrocatalytic performance for the CO<sub>2</sub>RR. This interaction not only enhances CO<sub>2</sub> adsorption and activation but also promotes favorable reduction pathways, leading to high-value product formation. The regulation of coordination environments has provided a theoretical and experimental basis for designing high-performance dual-metal catalysts, elucidating the mechanisms of metal interactions and improving overall catalytic efficiency. Therefore, the strategic design of coordination environments in dual-metal catalysts, through the careful selection of central metals, ligands, bridging atoms and other coordination parameters, is essential for achieving efficient and selective electrocatalytic CO<sub>2</sub> reduction.

## 2.2 Geometric structure regulation

Geometric structure regulation is another important aspect of dual-metal catalyst design. By controlling the crystal facet of the metal active sites, the catalyst can be optimized to facilitate the formation of desired products. The incorporation of a second metal can help stabilize these favorable crystal facets, thereby enhancing the catalyst's selectivity for specific products in CO<sub>2</sub> conversion. Additionally, the size of the nanoparticles used in CO<sub>2</sub> reduction can be controlled by the addition of a second metal. Smaller nanoparticles tend to increase the number of active sites and promote the catalytic performance. Morphology regulation is also crucial, as different morphologies such as polyhedra, nanosheets, hierarchical nanoflowers, and porous structures can exhibit unique physicochemical properties that affect the catalyst's performance. By carefully designing the morphology of the dual-metal catalysts through the addition of a second metal, the catalyst can be optimized for high selectivity towards the electrocatalytic CO<sub>2</sub>RR.<sup>85,86</sup>

**2.2.1 Crystal facet regulation.** The crystal facets of copper materials are regarded as the primary catalytic sites where the electrocatalytic CO<sub>2</sub>RR occurs. The type of crystal facets of copper materials can determine the adsorption energy of CO<sub>2</sub> reduction intermediates, thereby influencing the pathway of the catalytic CO<sub>2</sub> reduction process. Studies have demonstrated a strong correlation between the selectivity of electrocatalytic CO<sub>2</sub>RR products and the crystal facets of single-crystal Cu.<sup>87</sup> Specifically, the Cu (100) facet tends to favor the production of C<sub>2</sub>H<sub>4</sub>, whereas the Cu (111) facet exhibits higher selectivity toward CH<sub>4</sub>. In contrast, the Cu (110) facet shows a greater propensity for generating oxygenated hydrocarbons, such as CH<sub>3</sub>CH<sub>2</sub>OH and CH<sub>3</sub>COOH, compared to Cu (100) and Cu





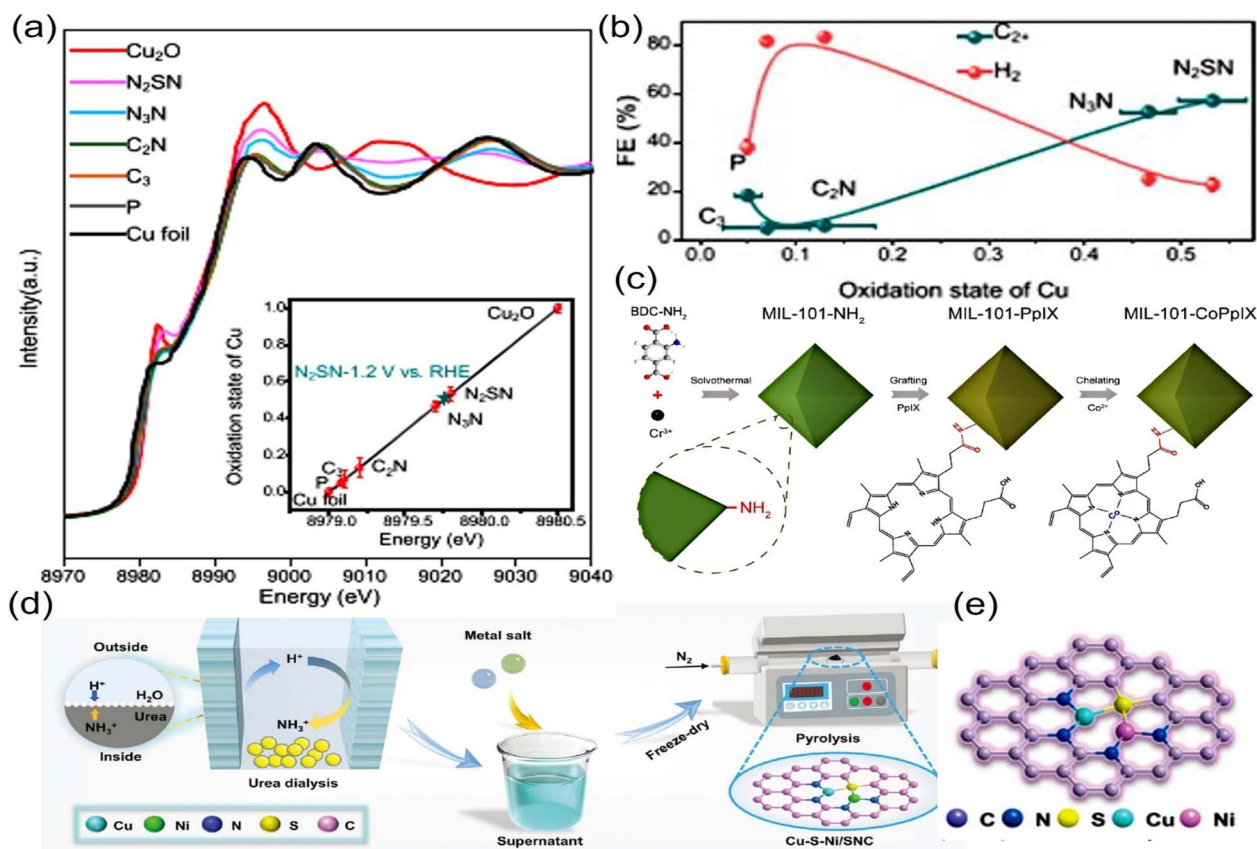


Fig. 3 (a) XANES spectra at the Cu K-edge of the Ag–Cu catalyst. (b) Evolution of the faradaic efficiency for  $C_{2+}$  and  $H_2$  measured at  $-1.2$  V vs. RHE with the oxidation state of Cu. (c) Synthesis of MIL-101-CoPpIX. (d) Schematic illustration of the synthesis of the Cu–S–Ni/SNC catalyst. (e) Schematic illustration of the synthesis of the Cu–S–Ni/SNC catalyst. (a and b) Reproduced with permission.<sup>80</sup> Copyright 2021, Springer Nature. (c) Reproduced with permission.<sup>81</sup> Copyright, 2024, Elsevier. (d and e) Reproduced with permission.<sup>84</sup> Copyright 2024, Wiley.

(111).<sup>88</sup> However, it is important to note that other byproducts are often generated simultaneously during these processes. To more precisely control the types of crystal facets during the design and synthesis process and further enhance the selectivity of these facets toward desired products, introducing a second metal into copper-based catalysts to form dual-metal catalysts has proven to be a highly effective strategy.<sup>89</sup>

In the design and preparation of dual-metal catalysts, controlling the crystal planes of metal active sites is a crucial step. This strategy focuses on selectively exposing crystal planes that are most favorable for specific chemical reactions, thereby enhancing catalytic performance and significantly promoting the formation of desired products. Specifically, introducing a second metal can stabilize the crystal planes conducive to target product formation, enabling the catalyst to exhibit higher selectivity—preferentially generating the desired product over by-products. The integration of crystal plane regulation with secondary metal incorporation offers an innovative framework for the development of efficient and highly selective catalysts. Fan, Huang, Xi *et al.* achieved well-defined Ag–Cu Janus nanostructures with {100} facets (JNS-100) through the confined growth of Cu on Ag nanocubes (NCs). The introduction of Ag into the Cu catalyst system created a synergistic catalytic effect. DFT calculations revealed that the electronic structure of Ag–Cu

JNS-100 was optimized due to the electron transfer from Ag to Cu domains, which enhanced the catalytic activity. The Ag domains efficiently converted  $CO_2$  to CO at lower overpotentials, while the generated CO then spilled over to the adjacent Cu domains, where it was further reduced and C–C coupling was realized toward  $C_2H_4$  production with high efficiency. This tandem mechanism, combined with the exposed {100} facets on the Cu domains, significantly improved the selectivity and efficiency of the  $CO_2$ RR toward  $C_{2+}$  products. Specifically, the  $Ag_{65}-Cu_{35}$  JNS-100 catalyst demonstrated a FE of 54% for  $C_2H_4$  and 72% for  $C_{2+}$  products at  $-1.2$  V (vs. RHE), outperforming pure Cu nanocubes and physical mixtures of Ag and Cu (Fig. 4a and b).<sup>90</sup> Zheng, Kuang *et al.* successfully incorporated the metal Mg into the Cu catalyst to promote the formation and stabilization of Cu (111) facets, which were particularly effective in promoting C–C coupling, and enhancing the production of ethanol with a high  $FE_{ethanol}$  of  $76.2 \pm 4.8\%$  at  $600\text{ mA cm}^{-2}$ . It was found that the Cu (111) facets provided a high density of active sites and optimal adsorption energies for key intermediates such as  $*CO$ . These facets also lowered the energy required for  $*CO-CO$  coupling, and improved the stabilization of the  $*CHCHOH$  intermediate, which were critical for ethanol production. Moreover, the synergistic effect between Cu and Mg in the dual-metal material

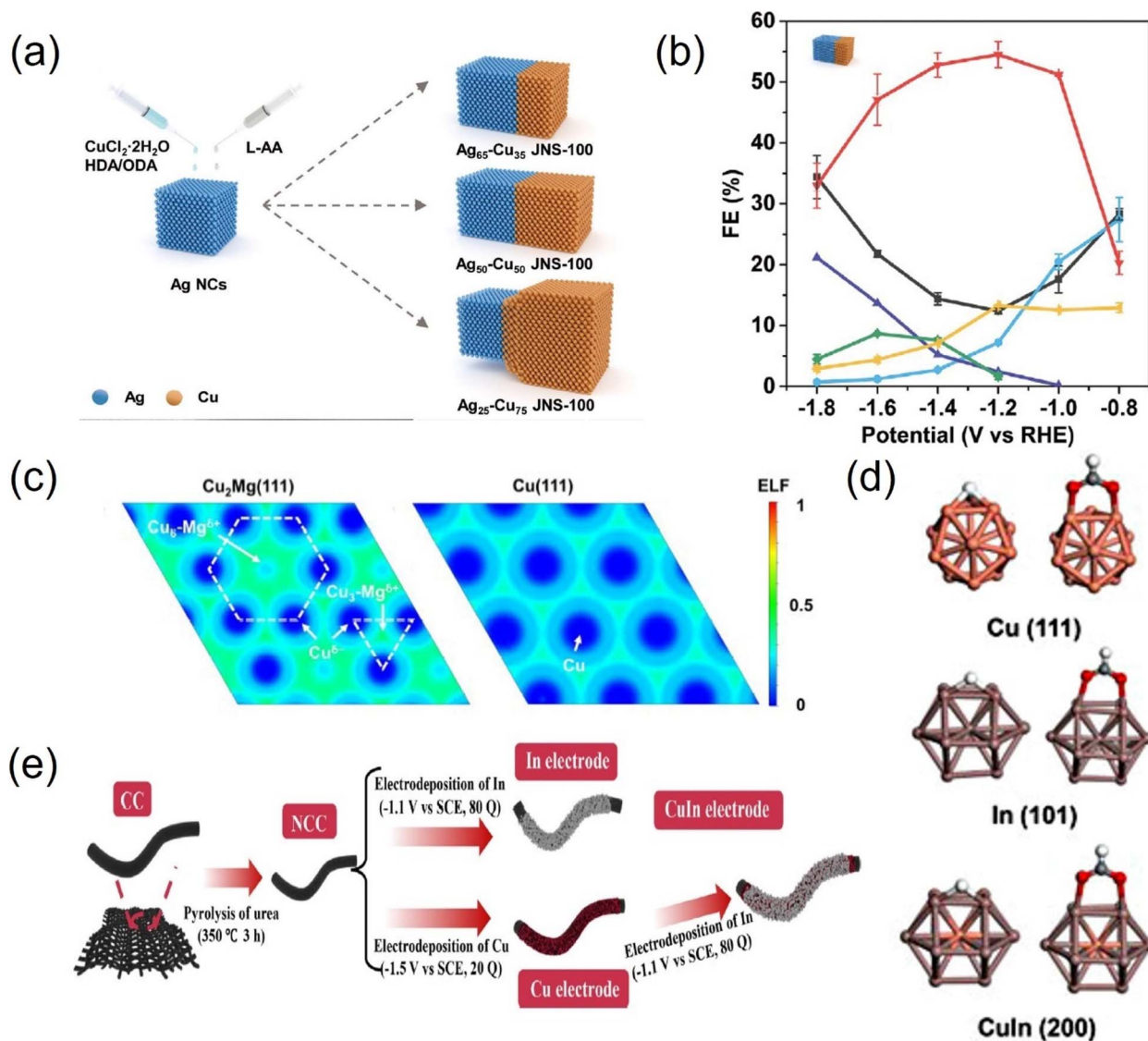


Fig. 4 (a) Schematic illustration for the synthesis of three kinds of Ag-Cu JNS-100. (b) Faradaic efficiencies (FEs) for  $\text{CO}_2\text{RR}$  products obtained on  $\text{Ag}_{65}\text{-Cu}_{35}$  JNS-100. (c) Electronic localization function of  $\text{Cu}_2\text{Mg}(111)$ . (d) Optimized structure of cluster  $\text{Cu}(111)$ , cluster  $\text{In}(101)$ , and cluster  $\text{CuIn}$  alloy (200). (e) Schematic diagram of the fabrication process of the CuIn electrode. (a and b) Reproduced with permission.<sup>90</sup> Copyright 2021, Wiley. (c) Reproduced with permission.<sup>91</sup> Copyright 2023, John Wiley and Sons Ltd. (d and e) Reproduced with permission.<sup>92</sup> Copyright 2023, Elsevier.

facilitated the electron transfer from Mg to Cu, leading to a negative shift in the d-band center compared to that of commercial Cu, indicating a more favorable electronic environment for C-C coupling (Fig. 4c).<sup>91</sup>

In addition to the conventional approach of modulating copper crystal facets, such as the (100) plane, the regulation of other types of metal facets through the synergistic effect of dual-metal systems is also considered as a promising approach for enhancing the electrocatalytic  $\text{CO}_2\text{RR}$ . Qiao, Zhang and their team developed CuIn dual-metal catalysts featuring co-exposed CuIn (200) and In (101) facets, which exhibited a high FE up to 80% for formate production at relatively low overpotentials, along with high stability. They discovered that the synergistic effect of the two metals played a crucial role, where the CuIn

(200) facet can specifically reduce the overpotential for formate production, while the In (101) facet can enhance the overall  $\text{CO}_2$  adsorption capacity. Density functional theory (DFT) calculations further revealed that the CuIn (200) and In (101) lattice facets collaborate to stabilize the key  $\text{OCHO}^*$  intermediate (Fig. 4d and e).<sup>92</sup> Xiong *et al.* achieved highly efficient electrocatalytic  $\text{CO}_2\text{RR}$  to produce formate by fabricating dual-metal  $\text{Bi}_5\text{In}_5$  nanofibers (NFs) with precise control over the growth of InBi (200) crystal facets, through a synthetic approach combining electrospinning and electrochemical reduction techniques. It was found that attributed to the dual-metal sites formed by In and Bi atom, the (200) crystalline plane of  $\text{Bi}_5\text{In}_5$  could promote the electrocatalytic  $\text{CO}_2\text{RR}$  process by strongly adsorbing the key  $\text{*OCHO}$  intermediate and reducing the



reaction energy barrier, thereby enhancing catalytic selectivity for HCOOH production.<sup>93</sup>

In summary, the precise regulation of crystal facets in dual-metal catalysts has emerged as a highly effective approach to enhance the selectivity and efficiency of electrocatalytic CO<sub>2</sub> reduction. By tailoring specific facets and leveraging synergistic effects in dual-metal systems, remarkable control over reaction pathways has been achieved, enabling high FE for target products. These advancements highlight the critical role of facet engineering in optimizing intermediate adsorption and lowering energy barriers for key steps.

**2.2.2 Size regulation.** The size of dual-metal catalysts such as dual-atoms, clusters and nanoparticles governs their electrocatalytic CO<sub>2</sub>RR performance by balancing atomic efficiency, intermediate binding, and reaction pathways.

As for dual-atom catalysts (DACs) consisting of two heterometallic active centers, they represent an emerging class of electrocatalysts that combine the advantages of single-atom catalysts (SACs) and subnanometer clusters for the CO<sub>2</sub>RR. By precisely engineering dual-metal sites, DACs can achieve maximized metal atom utilization while enabling synergistic electronic and geometric effects that are unattainable with isolated SACs or larger clusters.<sup>94</sup> Lu, Liu, *et al.* employed a molten-salt-assisted strategy to synthesize Fe–Zn dual-atom catalysts (FeZnNC) on N-doped carbon supports. The study demonstrated that due to the electronegativity difference between Fe and Zn (Fe: 1.83; Zn: 1.65), electrons preferentially transferred from Zn to Fe, which resulted in charge redistribution and modified electronic environments of the two active sites, creating optimal conditions for the CO<sub>2</sub>-to-CO conversion pathway. The synergistic effect of dual-atom catalysts entailed the Zn site functioning as the primary active center for CO<sub>2</sub> activation and \*COOH intermediate formation, with the Fe site stabilizing intermediates and weakening \*CO binding to avert site poisoning, thereby achieving FE<sub>CO</sub> > 94% in acidic media at industrial current densities ranging from 100 to 400 mA cm<sup>−2</sup> (Fig. 5a and b).<sup>95</sup> Wang *et al.* developed a heterodimetallic Co–Ni–N–C dual-atom catalyst with neighboring Co–Ni diatomic sites, which attained a remarkable CO yield rate of 53.36 mA mg cat.<sup>−1</sup>, along with an outstanding FE<sub>CO</sub> of 94.1%. DFT calculations have revealed that the Co–Ni synergistic catalysis mechanism for the CO<sub>2</sub>RR entails the effective activation of CO<sub>2</sub> at dual Co–Ni sites and also the formation of CO *via* optimized pathways where another CO<sub>2</sub> molecule undergoes reduction while a CO\* intermediate remains adsorbed at the site (Fig. 5c and d).<sup>96</sup>

The metal clusters bridge atomic and nanoscale catalysts, as their well-defined yet tunable structures – ranging from a few to dozens of metal centers – combine atomic-level precision with nanoparticle-like ensemble effects. They can offer superior metal utilization like atomic catalysts, while avoiding the low metal loading limitations of atomic catalysts. Moreover, their multinuclear active sites can mimic the selectivity of nanoparticles, enabling tailored control over the C–C coupling reaction pathway for the CO<sub>2</sub>RR. The dual-metal clusters can offer superior catalytic performance compared to their monometallic systems by synergistically integrating the properties of

different metal components, which can modify charge distribution and orbital hybridization, enabling precise optimization of intermediate binding energies for enhanced electrocatalytic CO<sub>2</sub>RR activity.<sup>97</sup> Zhu, Jin, Du, *et al.* precisely engineered the structures of dual-metal clusters (Au<sub>8</sub>Ag<sub>55</sub>, Au<sub>8</sub>Ag<sub>57</sub>, and Au<sub>12</sub>Ag<sub>60</sub>) with different sizes, which enabled tailored catalytic performance for the CO<sub>2</sub>RR by manipulating geometric properties at the atomic level. They discovered that the smaller Au<sub>8</sub>Ag<sub>55</sub> NC exhibits a distinctive charge segregation phenomenon, where electrons preferentially gather around the core Au atoms while inducing an electron-deficient condition on the outer Ag atoms. This reduction in electron density on the Ag atoms effectively diminishes the competition from the HER, thereby enhancing the CO<sub>2</sub>RR process (Fig. 5f).<sup>98</sup> Metal–organic frameworks (MOFs) are unique cluster-based materials, in which atomically precise metal clusters are interconnected by well-ordered organic ligands, enabling outstanding electrocatalytic CO<sub>2</sub>RR performance. Lu, Francisco, Han, Zhu, *et al.* successfully constructed a Cu–Ni dual-metal MOF cluster with an asymmetric structure modulated by a pyrazolate ligand, namely Cu<sub>1</sub>Ni–BDP, which achieved a high CO<sub>2</sub>-to-C<sub>2</sub>H<sub>4</sub> conversion with a FE of 52.7% along with great stability. DFT calculations revealed that electron transfer from Cu to Ni generates electron-deficient Cu and electron-rich Ni sites in the asymmetric Cu<sub>1</sub>Ni cluster. The unique asymmetric Cu–Ni electronic configuration creates synergistic effects that precisely modulate \*CO adsorption energy while reducing the activation barrier for \*COH–COH formation, thereby enabling exceptional CO<sub>2</sub> reduction performance (Fig. 5e).<sup>99</sup>

In addition to dual-metal atomic catalysts and dual-metal clusters, the size regulation of dual-metal nanoparticle catalysts also has a significant impact on electrocatalytic CO<sub>2</sub> reduction. Although bulkier nanoparticles suffer from decreased atomic utilization efficiency, the complex surface architecture containing multiple active site types can directly offer high catalytic performance towards the CO<sub>2</sub>RR. Chen, Feng, *et al.* innovatively designed dual-metal ZnO/Ag twinned-phase ultrasmall nanoparticles (≤3 nm) uniformly embedded in a nanoporous carbon matrix, achieving 60.9% energy conversion efficiency for CO production with exceptional stability over six days. They discovered that nanopore confinement ensures the small particle size of the catalysts, leading to high active site density and agglomeration resistance. DFT calculations revealed that the charge redistribution from Zn/Ag to O atoms preferentially stabilizes the \*COOH intermediate while energetically disfavoring competing HCOO\* and \*H pathways, resulting in highly selective (98.1%) CO production.<sup>100</sup> Byon, Yang, *et al.* developed a series of dual-metal Cu<sub>x</sub>Ir<sub>1−x</sub> alloy nanoparticles with a small size of about 1.6 nm, which could achieve unprecedented performance in CO<sub>2</sub>-to-*t*-BuOH conversion, delivering a FE of 14.8%—very high C<sub>4</sub> production. Studies revealed that the high C<sub>4</sub> selectivity arises from the synergistic Cu–Ir interaction, combined with the oxophilic nature of the Ir-rich surface, which stabilizes critical oxygen-bound intermediates (*e.g.*, CH<sub>2</sub>CHO\*, CH<sub>3</sub>CHO, and CH<sub>3</sub>CH<sub>2</sub>O) and thereby boosts CO<sub>2</sub> reduction efficiency.<sup>63</sup>



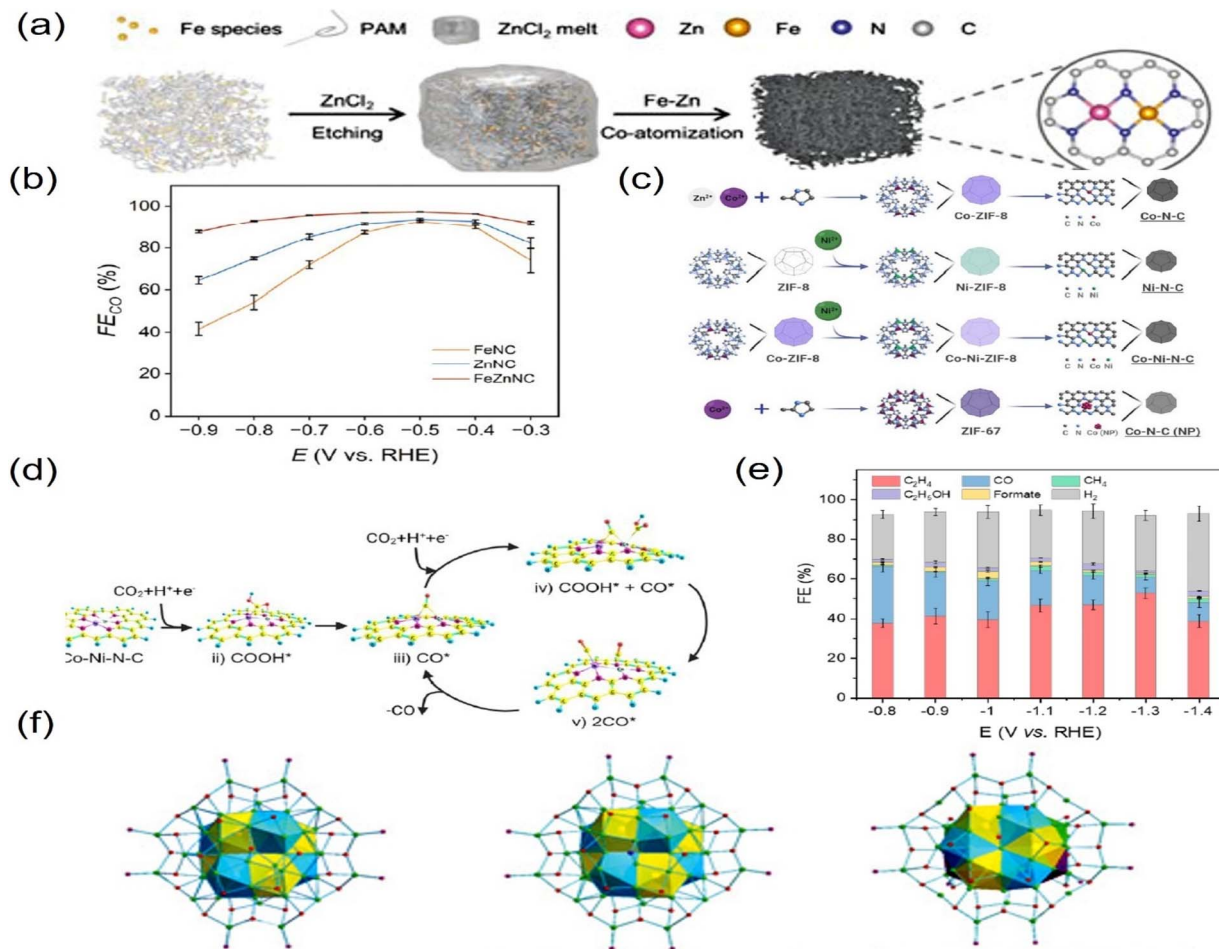


Fig. 5 (a) Scheme diagram for the synthesis of a dual-atom FeZnNC catalyst. (b) Faradaic efficiencies of CO at different potentials by using FeZnNC. (c) Schematic diagram of the fabrication process of Co-N-C, Ni-N-C, Co-Ni-N-C, and Co-N-C (NP) (NP: nanoparticle). (d) Catalytic pathway on the dual Co-Ni site based on the optimized structures of adsorbed intermediates COOH\* and CO\*. (e) Faradaic efficiencies for CO<sub>2</sub>RR products and H<sub>2</sub> on the Cu<sub>3</sub>Ni-BDP MOF at different cathode potentials. (f) Total structure of Au<sub>8</sub>Ag<sub>55</sub>, Au<sub>8</sub>Ag<sub>57</sub>, and Au<sub>12</sub>Ag<sub>60</sub> NC. (a and b) Reproduced with permission.<sup>95</sup> Copyright 2024, John Wiley and Sons Inc. (c and d) Reproduced with permission.<sup>96</sup> Copyright 2024, the Royal Society of Chemistry. (e) Reproduced with permission.<sup>99</sup> Copyright 2023, Wiley-VCH Verlag, Wiley. (f) Reproduced with permission.<sup>98</sup> Copyright 2023, American Chemical Society.

The size regulation of dual-metal catalysts is a powerful lever to tailor the synergistic effect on catalytic properties for the electrocatalytic CO<sub>2</sub>RR. The interplay of electronic and geometric effects across scales will drive advancements in high-performance CO<sub>2</sub>RR catalysts.

**2.2.3 Morphology regulation.** Morphological regulation is pivotal for designing efficient dual-metal catalysts for the electrocatalytic CO<sub>2</sub>RR. Precisely engineering morphological architectures, such as shape control and porous regulation could optimize surface area, active site accessibility, electronic interactions, and mass transport efficiencies, thereby offering unprecedented catalytic performance with superior activity, selectivity, and operational stability. The integration of morphological engineering and dual-metal composition optimization emerges as a pioneering strategy for designing catalysts that enable industrial-scale CO<sub>2</sub> conversion.<sup>101</sup>

By utilizing the modulation of two unique metals, dual-metal catalysts can be morphologically optimized into diverse

nanostructures, ranging from distinct shapes like polyhedra, nanosheets, hierarchical nanoflowers or dendrites, to porous structures like core-shell or hollow structures. This approach enhances mass transport efficiency and promotes electrolyte infiltration during the CO<sub>2</sub>RR by establishing directional charge/mass transfer pathways and increasing the surface area available for reactant interaction.<sup>102,103</sup>

Polyhedral structures in nanomaterials offer numerous advantages that make them highly attractive for various applications. The unique shape and arrangement of atoms in polyhedral nanomaterials often lead to tailored electronic properties and enhanced catalytic activity for the electrocatalytic CO<sub>2</sub>RR.<sup>104</sup> For instance, Zhang, Wang, and colleagues reported that the incorporation of Ag into Cu<sub>3</sub>N nanocubes (NCs) leads to a well-defined nanocube (NC) structure, where Ag atoms are successfully integrated into some Cu sites within the Cu<sub>3</sub>N unit cell, resulting in Cu<sub>3</sub>N-Ag NCs. The dual Ag-Cu sites exhibit a cascade catalysis strategy that markedly boosts the

electrochemical CO<sub>2</sub> reduction process, resulting in significantly enhanced FE and partial current density for C<sub>2</sub>H<sub>4</sub> production, which are much higher compared to those of pure Cu<sub>3</sub>N nanocubes (NCs). They discovered the synergistic effect between Cu and Ag, wherein the relatively weak binding strength of \*CO on Ag sites aids in the generation and subsequent transfer of CO species to Cu sites. At these Cu sites, the elevated local CO coverage promotes asymmetric C–C coupling, leading to the formation of key intermediate species \*COCHO (Fig. 6a).<sup>48</sup> In another example, Gong's group reported that incorporating dual-metal doping into catalytic materials presents a potent strategy for modulating their structural attributes and substantially impacting the efficiency of electrocatalytic CO<sub>2</sub> reduction. By adjusting the ratios of Cu and Pd precursors, diverse morphological transformations of Pd–Cu nanocrystals (NCs) can be realized, spanning from concave rhombic dodecahedra to flower-like structures. The flower-like Pd<sub>3</sub>Cu (FL-Pd<sub>3</sub>Cu), composed of {111} and high-index step facets, contributed to their high selectivity for CO production. Conversely, the concave rhombic dodecahedral Cu<sub>3</sub>Pd (CRD-Cu<sub>3</sub>Pd) exposed high-index facets, which have demonstrated a reduced onset potential and increased current density for CH<sub>4</sub> production compared to Cu foil. They discovered that attributed to the synergistic effects of Cu and Pd as well as the exposure of high-index facets, CRD-Cu<sub>3</sub>Pd offered more low coordinated active sites and modified the binding energies of reaction intermediates such as \*CHO, thereby enhancing its catalytic performance for CH<sub>4</sub> production (Fig. 6b).<sup>105</sup>

Due to their two-dimensional (2D) confinement and ultra-thin nature, nanosheets exhibit an enormously high surface area-to-volume ratio, which often leads to unique properties such as high carrier mobility and tunable band gaps, which are particularly advantageous for the electrocatalytic CO<sub>2</sub>RR.<sup>106,107</sup> Wang and Che's group reported that metals like Co, In and Ru were successfully introduced into Bi materials *via* a facile hydrolysis method, resulting in the formation of metal-doped Bi nanosheets with unique structural and chemical properties compared to pristine Bi nanosheets. Notably, the Co<sub>0.05</sub>–BOON nanosheets significantly enhanced the electrocatalytic reduction of CO<sub>2</sub> to HCOOH, thanks to the synergistic effect between cobalt and bismuth. The incorporation of cobalt atoms into the bismuth nanosheets modulated the electronic structure *via* electron transfer, leading to a high selectivity (~90%) and stability for HCOOH production over 100 hours at 100 mA cm<sup>−2</sup>. Moreover, the Co-doped Bi (012) surface exhibited stronger binding energy towards the key OCHO\* intermediates, facilitating the efficient conversion of CO<sub>2</sub> to formic acid at a lower applied potential compared to the pure Bi surface (Fig. 6d).<sup>108</sup> In another study, Zhang and colleagues reported on the CuMnO<sub>2</sub> nanosheet structure, wherein the controlled synthesis method introduced Cu and Mn, yielding a material abundant in oxygen vacancy defects. The abundant oxygen vacancies in the CuMnO<sub>2</sub>–Vo nanosheets effectively shift the d-band center of the active Mn sites upwards. The synergistic effect of Cu and Mn in the CuMnO<sub>2</sub> nanosheets, coupled with the presence of oxygen vacancies, significantly enhances the adsorption strength of the active sites for the intermediates \*COOH and

\*CO, resulting in a high FE for ethylene production (93.4% at −1.0 V vs. RHE) and excellent stability over 192 hours (Fig. 6c and e).<sup>109</sup>

The branching structure of dendrites and the layered petals of nanoflowers offer excellent mass transport pathways, which can facilitate the efficient diffusion of CO<sub>2</sub> to the active sites and the removal of reduction products from the catalyst surface, reducing mass transfer limitations and enhancing the overall reaction rate for the CO<sub>2</sub>RR.<sup>110–112</sup> Liu *et al.* reported that the integration of Cu and Sn into the Cu<sub>1</sub>SnS<sub>2</sub> catalyst leads to the formation of a unique microflower-like nanostructure, creating a hierarchical architecture with multiple layers and pores. The doping of Cu into SnS<sub>2</sub> not only modifies the electronic structure of the material but also plays a pivotal role in shaping its morphological features. The *operando* detections confirmed that the incorporation of a single Cu atom into the Cu<sub>1</sub>/SnS<sub>2</sub> catalyst could promote the reduction of SnS, resulting in the formation of Cu<sub>1</sub>/Sn during the CO<sub>2</sub>RR. This dynamic transformation effectively boosts the generation of CO<sub>2</sub><sup>−</sup>/OCHO intermediates. DFT calculation found that Cu<sub>1</sub> and Sn work together as active sites to reduce the Gibbs free energy for the formation of the \*OCHO intermediate, facilitating the conversion of CO<sub>2</sub> to formate (Fig. 6f).<sup>113</sup> In another example, Lu, Jiao, *et al.* constructed a Bi<sub>2</sub>O<sub>3–x</sub>/Mg(OH)<sub>2</sub> catalyst with a nanoflower-like structure, which can increase the surface area of the catalyst, providing more active sites for CO<sub>2</sub> adsorption and reduction even for low-concentration CO<sub>2</sub>. They discovered that the dual-active-site catalyst leverages a synergistic effect between the bismuth oxide active sites and the magnesium hydroxide basic sites, in which a Lewis-base active site can facilitate the enrichment and activation of CO<sub>2</sub>, along with a highly selective catalytic site dedicated to CO<sub>2</sub> conversion, leading to a high formic acid selectivity exceeding 97% across a wide potential range (Fig. 6g).<sup>114</sup> There are also many dual-metal catalysts with dendrite structures for the electrocatalytic CO<sub>2</sub>RR, which exhibit excellent catalytic performance. For instance, Schultz *et al.* reported a dual-metal catalyst Ag/Cu<sub>2</sub>O with dendritic morphology, in which the combination of Ag and Cu<sub>2</sub>O leads to selective photoelectrochemical CO<sub>2</sub> reduction to acetate, with a high FE of 54%. It was found that the Ag/Cu<sub>2</sub>O nanodendrite structure exhibits a unique combination of plasmonic and semiconductor properties that synergistically enhance the CO<sub>2</sub> reduction reaction. The *in situ* tests revealed that the reaction rate entails the transfer of a single electron from the electrode to CO<sub>2</sub>, leading to its reduction into the \*CO<sub>2</sub><sup>−</sup> radical anion and subsequently generating adsorbed CO, which acts as a vital intermediate in the process of C–C coupling for acetate production (Fig. 6i).<sup>115</sup>

The porous structures like core–shell or hollow structures can not only offer a larger surface area and more active sites compared to their bulk counterparts, but also enhance CO<sub>2</sub>/product diffusion, significantly reducing mass transfer limitations.<sup>116,117</sup> For instance, Zeng, Tuo, *et al.* developed a group of dual-metal Ag@Cu<sub>2</sub>O core–shell nanoreactors featuring adjustable Cu<sub>2</sub>O shell thicknesses, displaying a volcano-like pattern in the generation of C<sub>2+</sub> products, in which Ag@Cu<sub>2</sub>O-40 with medium thickness exhibited the highest FEC<sub>2+</sub> of





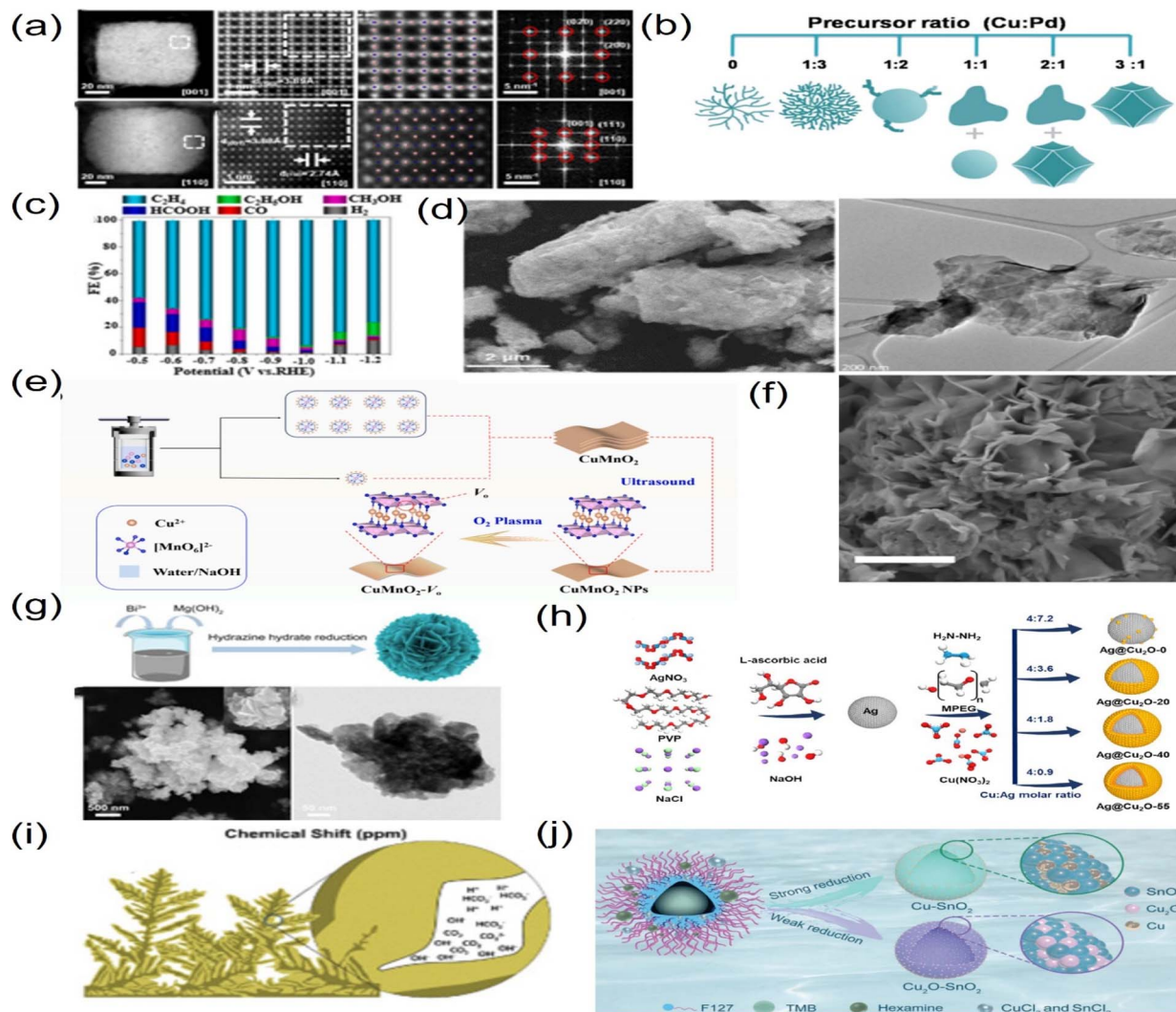


**Fig. 6** (a) Structural characterization of  $\text{Cu}_3\text{N}$ -Ag NCs. (b) Morphological evolution of Pd-Cu catalysts with different compositions. (c) Faradaic efficiencies for  $\text{CO}_2\text{RR}$  products by using  $\text{CuMnO}_2$ . (d) Structural characterization of  $\text{Co}_{0.05}$ -BOON. (e) Synthesis schematic of  $\text{CuMnO}_2$ -Vo. (f) SEM image of  $\text{Cu}_1/\text{SnS}_2$ . (g) Synthesis and characterization of dual-active site catalyst  $\text{Bi}_2\text{O}_{3-x}/\text{Mg}(\text{OH})_2$ . (h) Schematic illustration for the synthesis of  $\text{Ag}@\text{Cu}_2\text{O}$  cascade nanoreactors. (i) Representative scheme of the microenvironment of  $\text{Ag}/\text{Cu}_2\text{O}$  during the  $\text{CO}_2$  reduction process. (j) Schematic illustration for synthesizing Cu-Sn-based catalysts in the  $\text{CO}_2\text{RR}$ . (a) Reproduced with permission.<sup>48</sup> Copyright 2024, American Chemical Society. (b) Reproduced with permission.<sup>105</sup> Copyright 2017, Wiley-VCH Verlag. (c and e) Reproduced with permission.<sup>109</sup> Copyright, 2025, Elsevier. (d) Reproduced with permission.<sup>108</sup> Copyright 2024, John Wiley and Sons Ltd. (f) Reproduced with permission.<sup>113</sup> Copyright 2024, American Chemical Society. (g) Reproduced with permission.<sup>114</sup> Copyright 2025, Springer. (h) Reproduced with permission.<sup>103</sup> Copyright 2023, American Chemical Society. (i) Reproduced with permission.<sup>115</sup> Copyright 2024, American Chemical Society. (j) Reproduced with permission.<sup>118</sup> Copyright 2024, Wiley.

78.5%. The combination of Ag and  $\text{Cu}_2\text{O}$  in a core-shell structure leads to synergistic effects, in which the CO generated at the Ag core spills over to the  $\text{Cu}_2\text{O}$  shell, where it promotes the C-C coupling for  $\text{C}_{2+}$  production. They discovered that the porous  $\text{Cu}_2\text{O}$  shell creates a confined space around the Ag core, promoting the local accumulation of CO intermediates. Meanwhile, the short diffusion pathways between the Ag core and  $\text{Cu}_2\text{O}$  shell minimize the loss of reactive intermediates, ensuring efficient utilization of CO for subsequent C-C coupling (Fig. 6h).<sup>101</sup> As for the hollow structure, Sun, Zhang, *et al.* developed two dual-metal Cu-Sn oxide based catalysts  $\text{Cu-SnO}_2$  and  $\text{Cu}_2\text{O-SnO}_2$  with hollow spherical structures, of which

the former was obtained under strong reduction conditions, while the latter was obtained under weaker reduction conditions. The findings reveal that the  $\text{Cu-SnO}_2$  catalyst exhibits remarkable selectivity towards ethanol, achieving a selectivity of 74.6%, while the  $\text{Cu}_2\text{O-SnO}_2$  catalyst shows high selectivity towards ethylene, with a value of 71.4%. This underscores the crucial role played by the distinct interphases formed between Cu/ $\text{Cu}_2\text{O}$  and  $\text{SnO}_2$  in determining the product distribution, demonstrating a significant impact on the catalytic outcomes. DFT calculations uncovered that the  $\text{Cu-SnO}_2$  interphase features robust electron interactions, facilitating the generation of essential intermediates such as  $^*\text{COH}$ , which favors

**Table 1** Summary of state-of-the-art dual-metal catalysts for the electrocatalytic CO<sub>2</sub>RR into C<sub>1</sub> products

Catalyst	Dual metals	FE of C <sub>1</sub> products (%)	Current density $j_{C_1}$ (mA cm <sup>-2</sup> )	Electrolyte	Ref.
Vo-CuO(Sn)	Cu and Sn	99 (CO)	38.65	0.1 M KHCO <sub>3</sub>	71
Cu/CeO <sub>2</sub>	Cu and Ce	70.03 (CH <sub>4</sub> )	150	1 M KOH	63
Cu-ZnO	Cu and Zn	80 (CO)	45	0.1 M KHCO <sub>3</sub>	65
MIL-101-CoPpIX	Co and Cr	97.1 (CO)	5	0.1 M KHCO <sub>3</sub>	81
Cu-S-Ni/SNC	Cu and Ni	98.1 (CO)	550	0.5 M KHCO <sub>3</sub>	84
CuIn	Cu and In	80 (HCOOH)	13.84	0.5 M KHCO <sub>3</sub>	92
Bi <sub>5</sub> In <sub>5</sub>	Bi and In	96.8 (HCOOH)	250.9	0.1 M KHCO <sub>3</sub>	93
FeZnNC	Fe and Zn	94 (CO)	100	1 M KOH	95
Co-Ni-N-C	Co and Ni	94.1 (CO)	13.34	0.1 M KHCO <sub>3</sub>	88
Au <sub>8</sub> Ag <sub>55</sub>	Au and Ag	66 (CO)	23	0.5 M KHCO <sub>3</sub>	98
ZnO-Ag@UC	Zn and Ag	98.1 (CO)	22.3	0.5 M KHCO <sub>3</sub>	100
Pd-Cu	Cu and Pd	40.6 (CH <sub>4</sub> )	16.7	0.1 M KHCO <sub>3</sub>	105
Co <sub>0.05</sub> -BOOM	Co and Bi	~90 (HCOOH)	200	1 M KOH	108
Cu <sub>1</sub> /SnS <sub>2</sub>	Cu and Sn	~90.9 (HCOOH)	158	0.5 M KHCO <sub>3</sub>	113
Bi <sub>2</sub> O <sub>3-x</sub> /Mg(OH) <sub>2</sub>	Bi and Mg	97 (HCOOH)	140	0.5 M KHCO <sub>3</sub>	114
Ni <sub>2</sub> -NCNT	Ni and Ni	97 (CO)	76	0.5 M KHCO <sub>3</sub>	126
Ni <sub>2</sub> /N-CNTs	Ni and Ni	90.7 (CO)	64.5	0.5 M KHCO <sub>3</sub>	118
Fe <sub>2</sub> -N-C	Fe and Fe	80 (CO)	32.04	0.5 M KHCO <sub>3</sub>	128
Ni-Cu	Cu and Ni	~99 (CO)	235	Phosphate buffer, 1 M KOH and 0.5 M KHCO <sub>3</sub>	122
Co-Cu DASC	Cu and Co	99.1 (CO)	483	0.5 M KHCO <sub>3</sub>	132

**Table 2** Summary of state-of-the-art dual-metal catalysts for the electrocatalytic CO<sub>2</sub>RR into C<sub>2+</sub> products

Catalyst	Dual metals	FE of C <sub>2+</sub> products (%)	Current density $j_{C_{2+}}$ (mA cm <sup>-2</sup> )	Electrolyte	Ref.
Cu <sub>x</sub> Ir <sub>1-x</sub>	Cu and Ir	14.8 ( <i>t</i> -BuOH)	0.207	0.1 M KHCO <sub>3</sub>	63
Cu/CaCO <sub>3</sub>	Cu and Ca	83.7	393	1 M KOH	64
Li <sub>2</sub> CuO <sub>2</sub>	Cu and Li	90.6	706	1 M KOH	73
Ag-Cu	Cu and Ag	80	261.1	0.5 M KHCO <sub>3</sub>	81
Ag <sub>65</sub> -Cu <sub>35</sub> JNS-100	Cu and Ag	72	15.14	0.1 M KHCO <sub>3</sub>	90
Cu <sub>2</sub> Mg(111)	Cu and Mg	76.2	720	1 M KOH	91
Cu <sub>1</sub> Ni-BDP	Cu and Ni	52.7	500	1 M KOH	99
Cu <sub>3</sub> N-Ag	Cu and Ag	36.6	26.7	1 M KOH	48
CuMnO <sub>2</sub>	Cu and Mn	93.4	14.57	0.1 M KHCO <sub>3</sub>	109
Ag@Cu <sub>2</sub> O-40	Cu and Ag	78.5	20	1 M KOH	103
Cu/Cu <sub>2</sub> O-SnO <sub>2</sub>	Cu and Sn	74.6	8.7	0.1 M KHCO <sub>3</sub>	118
Cu <sub>2</sub>	Cu and Cu	51	496.4	1 M KOH	122
BiCu-SAA	Cu and Bi	73.4	400	1 M KOH	140
Cu <sub>x</sub> Ga <sub>x</sub>	Cu and Ga	83	1000	1 M KOH and 0.5 M KHCO <sub>3</sub>	141
CoCu composite	Cu and Co	71.1	26.7	0.1 M KHCO <sub>3</sub>	52
CuO + Ni-surface	Cu and Ni	55.2	199	0.1 M KHCO <sub>3</sub>	62
B-Cu-Zn	Cu and Zn	79	200	1 M KOH	60
Ag/Cu <sub>2</sub> O-Cu	Cu and Ag	76.5	1000	1 M KOH	145
Cu/Ag	Cu and Ag	~80	356.7	1 M KOH	136
Au-Cu Janus NSs	Cu and Au	67	290	3 M KOH	149

asymmetric C-C coupling to yield ethanol. Conversely, the Cu<sub>2</sub>O-SnO<sub>2</sub> interphase is characterized by the presence of oxygen vacancies at both sites, enhancing the abundance of \*CO intermediates, thereby promoting symmetric C-C coupling to produce ethylene (Fig. 6j).<sup>118</sup>

Precise morphological control in dual-metal catalysts—ranging from polyhedra and nanosheets to hierarchical and porous architectures—enables tailored electronic and geometric effects that govern intermediate binding, C-C coupling, and mass transport. This structural diversification, coupled with synergistic metal interactions, paves the way for industrial-scale CO<sub>2</sub> conversion with target-product selectivity.

### 3 Influence of different types of dual-metal active sites with synergistic effects on the mechanism

The incorporation of dual-metal active sites in catalysts represents a highly effective strategy for enhancing catalytic performance, particularly in the field of electrocatalytic CO<sub>2</sub> reduction (Tables 1 and 2). The synergistic interactions between dual-metal sites can optimize reaction pathways, significantly improving catalytic activity, selectivity, and stability. Based on the size scale and structural characteristics of the active sites,



dual-metal active sites can be categorized into dual-atom metal catalysts and dual-metal nanoparticle catalysts.<sup>119</sup>

Dual-atom metal catalysts are composed of two isolated metal atoms, typically anchored on supports such as nitrogen-doped carbon or metal-organic frameworks. Their catalytic performance is finely tuned through electronic coupling and spatial proximity. The catalytic mechanism relies on atomic-level precision and the synergistic effects of dual-metal sites, particularly electronic synergy, which optimizes the adsorption of intermediates by modulating the d-band center. Specifically, electron transfer between the two metal atoms shifts their respective d-band centers, fine-tuning the adsorption strength: for instance, an upward shift in the d-band center of one metal atom enhances adsorption, while the other balances the adsorption strength through electron transfer or orbital hybridization, preventing efficiency loss caused by excessively strong or weak adsorption. In contrast, dual-metal nanoparticle catalysts feature active sites at the nanoscale (1–100 nm), with their catalytic performance governed by a combination of electronic effects, geometric effects, and interface effects. These include the optimization of intermediate adsorption through surface modification and electron transfer. Dual-atom metal catalysts demonstrate high selectivity in reduction reactions, predominantly yielding single products such as CO, while dual-metal nanoparticle catalysts are better suited for complex reactions, enabling the reduction of CO<sub>2</sub> to a variety of hydrocarbons.<sup>120</sup>

### 3.1 Dual-atom metal synergistic catalysis for the electrocatalytic CO<sub>2</sub>RR

Dual-atom catalysts (DACs), characterized by their exceptional atomic efficiency, precisely defined electronic structures, and unique dual-atom synergistic effects, have risen as prominent candidates for electrocatalytic CO<sub>2</sub> reduction. The precise arrangement of two metal atoms in DACs can create specific catalytically active sites with synergistic effects, which can lower the activation energy of the reaction, thereby accelerating the rate of CO<sub>2</sub> reduction. DACs can be further distinguished into homonuclear and heteronuclear types, each offering unique advantages for their applications for the electrocatalytic CO<sub>2</sub>RR. Hence, in this section, we will explore the impact of synergistic catalysis between dual metal atoms on the efficiency and catalytic mechanism of electrocatalytic CO<sub>2</sub> reduction, highlighting the distinct roles of homonuclear and heteronuclear dual-metal configurations.<sup>43</sup>

**3.1.1 Homo-dual atom synergistic catalysis.** Homonuclear dual-atom catalysts (DACs) have emerged as a groundbreaking class of materials in electrocatalytic CO<sub>2</sub> reduction, demonstrating superior catalytic performance compared to their single-atom counterparts. This enhanced performance is primarily attributed to the cooperative effects between dual metal active sites, which enable precise control over reaction pathways and intermediate stabilization.<sup>121</sup> The present study focuses on structural optimization through strategic regulation of metal types like Ni<sub>2</sub>, Fe<sub>2</sub>, Cu<sub>2</sub> and their coordination environments, aiming to achieve efficient conversion of CO<sub>2</sub> into CO

or hydrocarbons.<sup>122,123</sup> The synergistic mechanism of homonuclear DACs operates through a dual modulation of electronic and geometric effects, playing a pivotal role in determining the adsorption strength of key intermediates of CO<sub>2</sub> reduction.

Nickel, with its moderate d-band center position and rich valence state variability, is an ideal candidate for constructing highly efficient CO<sub>2</sub> reduction catalysts. Particularly in homonuclear dual-atom configurations, the synergistic interaction between two nickel atoms creates a uniform and consistent electronic effect, significantly enhancing catalytic performance. In this research direction, Lu's group has made systematic contributions. Among the pioneering studies in this field, Lu and colleagues achieved a significant breakthrough for the electrocatalytic CO<sub>2</sub>RR in 2018 with the development of a dinuclear nickel complex, Ni<sub>2</sub>L<sub>1</sub> (L<sub>1</sub> = 1,2-bis((5,7-dimethyl-1,4,8,11-tetra-azacyclotetradecan-6-yl)methyl)benzene). This catalyst demonstrated remarkable performance in CO<sub>2</sub> reduction, achieving a FE<sub>CO</sub> of 95%, a turnover number (TON) of 4.1 × 10<sup>6</sup>, and an impressive turnover frequency (TOF) of 190.0 s<sup>−1</sup>. The outstanding performance of complex Ni<sub>2</sub>L<sub>1</sub> compared to mononuclear Ni molecular catalysts for the CO<sub>2</sub>-to-CO conversion stems from the synergistic catalytic effect between its two Ni centers. It was found that one Ni center can serve as a Lewis base, donating an electron to the CO<sub>2</sub> molecule, while the other Ni center acts as a Lewis acid, stabilizing the partial negative charges on the O atom of CO<sub>2</sub>. This synergistic interaction significantly enhances the efficient conversion of CO<sub>2</sub> into CO. These findings underscore the promising potential of dual-metal synergistic catalysis in the field of electrochemical CO<sub>2</sub> reduction, establishing a new benchmark for deepening our understanding of the intricate structure-effect relationship (Fig. 7a).<sup>124</sup> Building upon this foundation, Lu's group made substantial progress in understanding the synergetic effects in dual-metal catalysts. In 2022, they systematically investigated three Ni<sub>2</sub> DACs, Ni<sub>2</sub>-N<sub>7</sub>, Ni<sub>2</sub>-N<sub>5</sub>C<sub>2</sub> and Ni<sub>2</sub>-N<sub>3</sub>C<sub>4</sub> with distinct coordination environments, identifying Ni<sub>2</sub>-N<sub>3</sub>C<sub>4</sub> as the most effective configuration for CO<sub>2</sub> reduction. The synergistic effect between the dual Ni centers in Ni<sub>2</sub>-N<sub>3</sub>C<sub>4</sub>, enabled by the fine-tuning of its electronic structure, plays a pivotal role in optimizing the binding energies to the COOH\* and CO\* intermediates, leading to the superior electrocatalytic CO<sub>2</sub>-to-CO reduction performance. This finding emphasizes the paramount importance of electronic structure modulation in the design of dual-atom catalysts (Fig. 7b).<sup>125</sup> Further advancements were made in 2023 with the synthesis of a uniform Ni<sub>2</sub>-NCNT catalyst loaded on N-doped carbon nanotubes (NCNT), demonstrating an outstandingly high FE exceeding 90% for CO production across a wide range of potentials, accompanied by a significant partial current density for CO, which is much higher than that of single-atom catalyst Ni<sub>1</sub>-NCNT. DFT calculations revealed that the synergistic interaction between the two Ni atoms in the Ni<sub>2</sub>-NCNT configuration effectively stabilizes the \*COOH intermediate and significantly reduces the free energy change in the rate-determining step when compared to the Ni<sub>1</sub>-NCNT SAC, thereby enhancing CO<sub>2</sub> reduction efficiency (Fig. 7c and d).<sup>126</sup> The most recent achievement of Lu's group in 2024 involved strategic coordination environment optimization





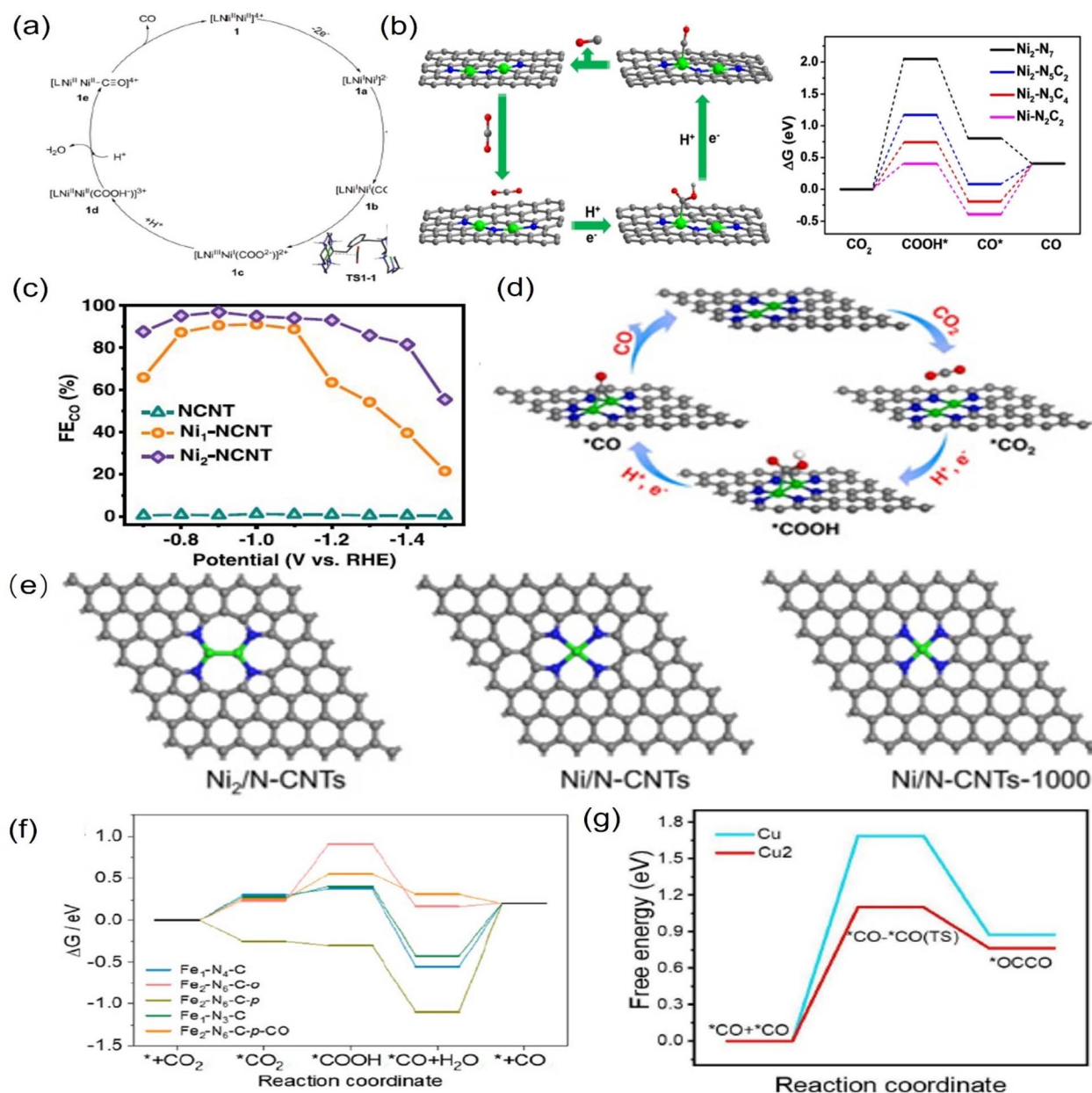


Fig. 7 (a) Mechanism for the conversion of CO<sub>2</sub> to CO, facilitated by a dinuclear nickel complex. (b) DFT calculations of Ni<sub>2</sub>N<sub>3</sub>C<sub>4</sub>. (c) Faradaic efficiencies of CO for NCNT, Ni<sub>1</sub>-NCNT and Ni<sub>2</sub>-NCNT catalysts. (d) Pathways of Ni<sub>2</sub>-N<sub>3</sub> (Ni<sub>2</sub>-NCNT) for CO<sub>2</sub> electroreduction to CO. (e) The optimized structures of Ni<sub>2</sub>/N-CNTs, Ni/N-CNTs, and Ni/N-CNTs-1000 (Ni<sub>2</sub>/N-CNTs-1000). (f) The free energy diagram of the CO<sub>2</sub>RR for Fe<sub>1</sub>-N<sub>4</sub>-C, Fe<sub>2</sub>-N<sub>6</sub>-C-o, Fe<sub>2</sub>-N<sub>6</sub>-C-p, Fe<sub>1</sub>-N<sub>3</sub>-C, and Fe<sub>2</sub>-N<sub>6</sub>-C-p-CO. (g) The energy barrier of Cu and Cu<sub>2</sub>. (a) Reproduced with permission.<sup>124</sup> Copyright 2017, the Royal Society of Chemistry. (b) Reproduced with permission.<sup>125</sup> Copyright 2022, John Wiley and Sons Ltd. (c and d) Reproduced with permission.<sup>126</sup> Copyright 2023, Elsevier. (e) Reproduced with permission.<sup>127</sup> Copyright 2025, Springer. (f) Reproduced with permission.<sup>128</sup> Copyright 2022, American Chemical Society. (g) Reproduced with permission.<sup>129</sup> Copyright 2024, John Wiley and Sons Ltd.

of Ni<sub>2</sub> dual-atoms through pyrrolic-N modification. They discovered that the pyrrolic-N-coordinated Ni<sub>2</sub> catalysts showcase markedly enhanced electrocatalytic performance in the conversion of CO<sub>2</sub> to CO, outperforming pyridinic-N-coordinated low-valent Ni catalysts. This significant advancement primarily stems from the fact that the intrinsically weak electron-donating characteristic of pyrrolic-N facilitates the formation of a reduced active site, which is extremely advantageous for the CO<sub>2</sub> electroreduction reaction. It was found that

the reaction free energy pertaining to \*COOH formation is notably lower on pyrrolic-N-coordinated Ni<sub>2</sub> catalysts in contrast to their pyridinic-N-coordinated Ni counterparts. Furthermore, the water molecules bound to the catalyst during the catalytic process are conducive to the formation of the key intermediate \*COOH and the desorption of CO, which greatly enhances the catalytic efficiency (Fig. 7e).<sup>127</sup>

Advancements in dual-atom catalysts were notably achieved by Han, Lee, and their collaborators in the realm of iron-based

catalysis. They engineered dual-atom Fe<sub>2</sub> sites within the Fe<sub>2</sub>-N<sub>6</sub>-C catalyst, achieving a FE for CO production exceeding 80% over an extended range of applied potentials, in contrast to their single-atom Fe<sub>1</sub>-N<sub>4</sub>-C counterparts. The orbital coupling between the two adjacent Fe atoms in the Fe<sub>2</sub> sites facilitates electron delocalization and reduces the energy levels of the Fe-3d orbitals. This phenomenon enables charge transfer between the Fe atoms and the CO intermediate during \*CO adsorption, thereby modulating the \*CO binding energy and promoting CO desorption (Fig. 7f).<sup>128</sup> Another achievement was made by He, Wang *et al.*, who developed a novel copper-based metal-organic polyhedral dual-atom catalyst Cu<sub>2</sub>, featuring a Cu-Cu bond distance of 2.95 Å, which demonstrated unprecedented C<sub>2</sub>H<sub>4</sub> production performance in 1.0 M KOH solution. The catalyst achieved a FE of 51% and a current density of 450 mA cm<sup>-2</sup>, significantly outperforming both Cu single-atom catalysts and Cu nanoparticles. Mechanistic studies revealed that the unique Cu atom pairs in the catalyst can modulate \*CO adsorption energy, promote C-C dimerization, and stabilize the \*OCCO intermediate, thereby dramatically enhancing C<sub>2</sub>H<sub>4</sub> production efficiency (Fig. 7g).<sup>129</sup>

These comprehensive studies have systematically elucidated the critical role of homonuclear dual-atom synergistic effects and coordination environment modulation in CO<sub>2</sub> electrocatalysis. The cooperative interaction between identical metal atoms optimizes reaction pathways, stabilizes key intermediates, and enhances catalytic performance in CO<sub>2</sub> reduction.

**3.1.2 Hetero-dual atom synergistic catalysis.** Heteronuclear dual-atom catalysts (DACs), composed of two distinct metal atoms, are a highly promising class of materials in the electrocatalytic CO<sub>2</sub>RR due to their exceptional synergistic effects arising from unique electronic and geometric properties.<sup>130</sup> Many kinds of DACs like Ni-Ag, Cu-Co, Cu-Ni, Cu-Te and Ni-Co have been explored for the electrocatalytic CO<sub>2</sub>RR. These catalysts mentioned above exhibit enhanced performance primarily through the electronic synergy includes charge transfer, polarization effects, and d-band center modulation. Heteronuclear DACs for the CO<sub>2</sub>RR can be categorized into two types based on the distance between the two distinct metal centers: those with closely spaced metal atoms forming direct metal-metal (M-M) bonds, and those without significant M-M interactions. Through comprehensive experimental studies coupled with theoretical calculations, heteronuclear DACs have demonstrated significant potential for designing highly efficient and selective CO<sub>2</sub> reduction catalysts, offering critical support for achieving sustainable energy conversion and carbon neutrality goals. The presence of M-M bonds in heteronuclear DACs introduces unique electronic and geometric effects that profoundly influence their electrocatalytic CO<sub>2</sub>RR performance. The formation of M-M bonds can facilitate orbital overlap leading to electron delocalization and modified d-band centers, which optimizes the adsorption strength of key intermediates like \*COOH and \*CO and lowers activation barriers for critical steps. Furthermore, in heteronuclear pairs, the electronegativity difference between metals induces charge asymmetry, where one metal acts as an electron donor (Lewis base) while the other serves as an electron acceptor (Lewis acid).<sup>131</sup> This cooperative

effect enhances CO<sub>2</sub> activation by stabilizing charged intermediates. Han, Sun *et al.* reported Cu-Ni heteronuclear DACs with Cu-Ni bonds, which exhibited exceptional CO selectivity across all pH conditions, achieving a near-universal FE<sub>CO</sub> of approximately 99% in acidic, neutral, and alkaline electrolytes. A particularly striking finding is the superior CO<sub>2</sub> utilization efficiency in acidic media (64.3%), which doubles the performance observed under alkaline conditions. Mechanistic investigations reveal strong electronic coupling between the Ni and Cu atomic sites, in which Cu acts as an electron donor to its neighboring Ni atom, leading to pronounced electron accumulation at Ni. Specifically, the Cu atoms induce an upward shift in the Ni d-band center position relative to the Fermi level, which thermodynamically favors and kinetically accelerates the critical \*COOH intermediate formation step (Fig. 8a).<sup>75</sup> In another study, Wu, Chen and colleagues successfully developed CoCu heteronuclear DACs featuring direct Co-Cu bonding, achieving high-density Co-Cu atomic pairs with strong inter-metallic interactions. DFT calculations show that the Co-Cu bond pushes the Co d-band center closer to the Fermi level, while the Cu d-band center remains deep. This tailored electronic structure balances intermediate adsorption strength, leading to industrial-scale current density for CO<sub>2</sub>-to-CO conversion with high selectivity. They discovered that the Co/Cu diatomic design synergistically addresses the limitations of single-atom catalysts by simultaneously lowering the energy barrier for \*COOH formation, a challenge for Cu-SACs, while weakening \*CO binding, a limitation of Co-SACs, thereby creating an optimized thermodynamic pathway (Fig. 8b and c).<sup>132</sup> Xu's group developed a Ni-Ag dual-atom catalyst (Ni-Ag/PC-N) with Ni-Ag bonded pairs supported on nitrogen-rich porous carbon, achieving an exceptional FE<sub>CO</sub> exceeding 90% across a wide potential range, with a peak efficiency of 99.2%. This outstanding activity stems from the synergistic interplay between Ni and Ag atoms, mediated by their metal-metal bonding and electronic interactions, which modulate the d-band centers of both metals and optimize intermediate adsorption/desorption energetics. Mechanistic investigations demonstrated that in the Ni-Ag DACs, the Ni site lowers the energy barrier for the formation of the \*COOH intermediate, whereas the Ag site alleviates catalyst poisoning induced by \*CO adsorption, ultimately leading to a synergistic enhancement of performance.<sup>133</sup>

Recent advancements in hetero-DACs without M-M bonds have also revealed remarkable synergistic catalytic effects in CO<sub>2</sub> reduction, with multiple research teams developing high-performance catalysts through innovative design and synthesis strategies. Lu, Jiao, *et al.* reported a TeN<sub>2</sub>-CuN<sub>3</sub> heteronuclear DAC with asymmetric coordination environments, offering a wide potential window for a high FE for CO production accompanied by enhanced reaction kinetics. It was confirmed that the Te center facilitates the activation of CO<sub>2</sub>, while the Cu center aids in the dissociation of H<sub>2</sub>O. Both experimental and theoretical findings indicate that the TeN<sub>2</sub>-CuN<sub>3</sub> configuration can collaboratively reduce the energy barriers associated with the rate-limiting step, thereby enhancing proton transfer kinetics (Fig. 8d).<sup>40</sup> In another



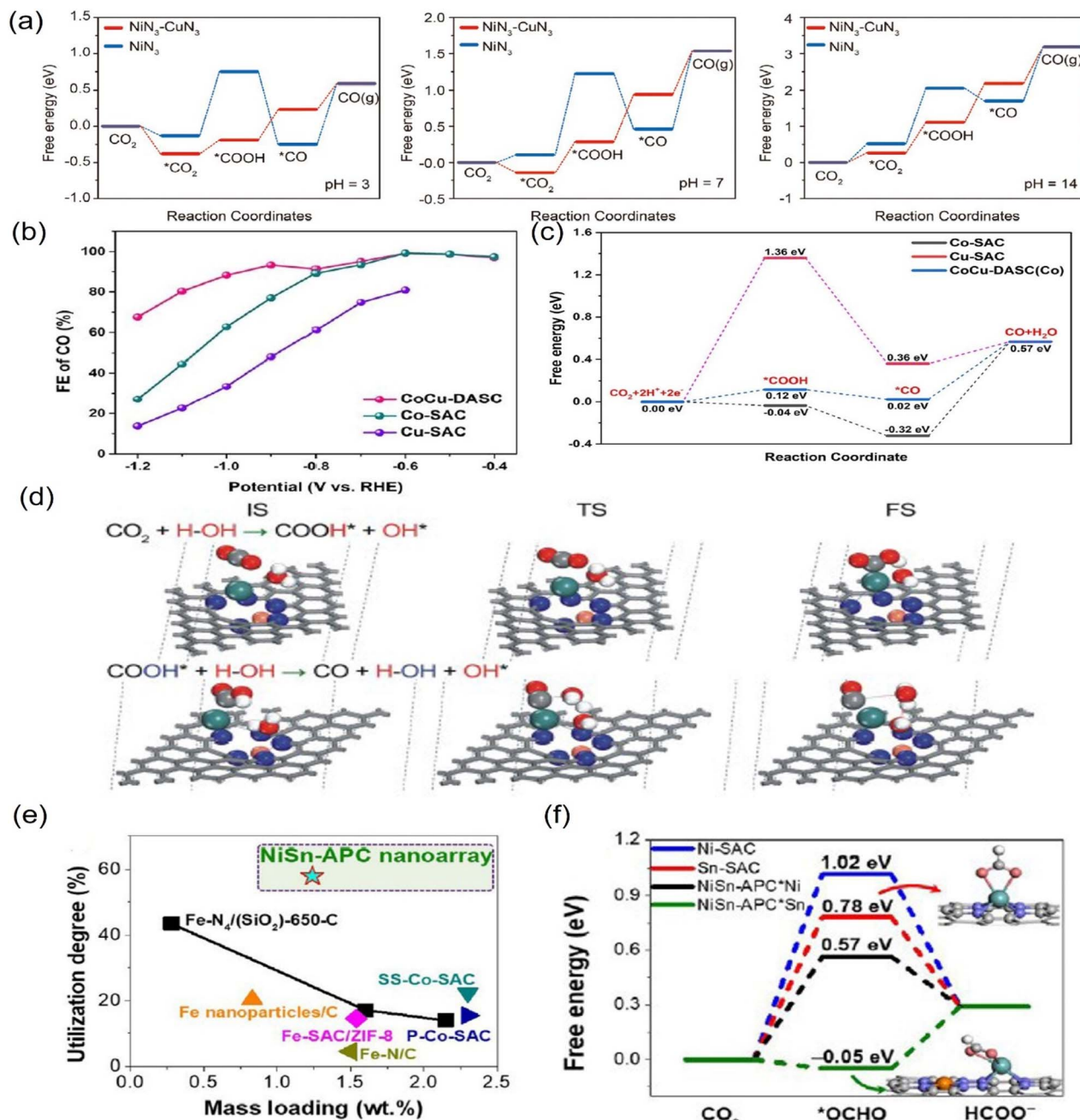


Fig. 8 (a) DFT calculations of NiN<sub>3</sub>-CuN<sub>3</sub> and NiN<sub>3</sub>. (b) faradaic efficiencies of CO measured in a H-type cell. (c) Free energy profiles of the CO<sub>2</sub>RR on CoCu-DASC Co-SAC and Cu-SAC. (d) Calculated configurations for the conversions of CO<sub>2</sub> → COOH\* and COOH\* → CO (IS, initial state; TS, transition state; FS, final state) over TeN<sub>2</sub>-CuN<sub>3</sub> DAC. (e) A comparative study on the utilization degree of various materials. (f) Free energy diagrams of the CO<sub>2</sub>RR for production of formate. (a) Reproduced with permission.<sup>75</sup> Copyright 2023, Wiley. (b and c) Reproduced with permission.<sup>132</sup> Copyright 2022, John Wiley and Sons Ltd. (d) Reproduced with permission.<sup>40</sup> Copyright, 2023, Springer Nature. (e and f) Reproduced with permission.<sup>134</sup> Copyright 2021, John Wiley and Sons Ltd.

example, Wei, Shao, *et al.* constructed a NiSn DAC featuring adjacent Ni and Sn atoms, each bonded to four nitrogen atoms, forming a N<sub>4</sub>-Ni-Sn-N<sub>4</sub> configuration. The fabricated NiSn DAC showcased exceptional efficiency in the conversion of CO<sub>2</sub> to formate *via* the CO<sub>2</sub>RR, attaining a remarkable TOF of 4752 h<sup>-1</sup>. It was found that the neighboring Ni-N<sub>4</sub> configuration could facilitate electron redistribution within the Sn atom, with the

synergistic catalytic effect leading to the lowered energy barrier for \*OCHO key intermediate formation (Fig. 8e and f).<sup>134</sup>

In summary, recent advancements in heteronuclear DACs for CO<sub>2</sub> reduction have demonstrated significant potential in achieving high efficiency and selectivity. Both DACs with M-M bonds and those without exhibit remarkable synergistic effects, which are primarily attributed to their unique electronic



configurations. The presence of M–M bonds facilitates orbital overlap, electron delocalization, and modified d-band centers, optimizing the adsorption strength of key intermediates and lowering activation barriers. In contrast, DACs without M–M bonds often rely on asymmetric coordination environments or specific atomic pairings to enhance catalytic performance.

### 3.2 Dual-metal nanoparticle synergistic catalysis for the electrocatalytic CO<sub>2</sub>RR

Copper is widely regarded as one of the most promising candidates for the electrocatalytic CO<sub>2</sub>RR due to its suitable adsorption capacity for reaction intermediates. However, the performance of Cu-based catalysts is often limited by issues such as poor selectivity, low activity, and rapid deactivation. These challenges necessitate the development of advanced strategies to enhance their catalytic performance. One effective strategy to overcome these limitations involves modifying copper-based nanoparticle catalysts by incorporating a secondary metal into the system. The electronic coupling between Cu and the secondary metal can modulate the electronic density of states, facilitating the charge transfer between the catalyst and reactants.<sup>135</sup> Most importantly, this approach can generate dual-active sites, creating a synergistic catalytic effect that enhances the overall catalytic performance.

In this section, the main focus is on leveraging the synergistic effects between the copper host and guest metals to tune the electronic and geometric structures of the resulting nanoparticle catalysts. By modifying the dual-active sites, the catalytic performance can be significantly improved. A wide range of guest metals, encompassing main-group metals, non-precious transition metals, noble metals, and lanthanides, will be extensively studied as secondary metals incorporated into Cu-based catalysts to explore their potential for enhancing the product efficiency of the CO<sub>2</sub>RR. A particular focus will be placed on elucidating the mechanisms underlying synergistic catalysis in the context of the CO<sub>2</sub>RR. Understanding these cooperative mechanisms holds immense significance to elucidate the structure–activity relationships and identify the key factors that govern their catalytic performance.

**3.2.1 Copper and main group metals.** Main-group metal elements, such as tin (Sn), bismuth (Bi), aluminum (Al), gallium (Ga), and indium (In), offer unique opportunities for modulating the electronic and geometric properties of copper-based nanomaterials. When main group metal elements are doped into copper, the p-electrons of the main group metal elements can hybridize with the d-electrons of copper. This hybridization leads to changes in the energy levels and distribution of electrons in the catalyst. In recent years, substantial progress has been achieved in the field of research focused on integrating main group metals into copper-based catalysts for the CO<sub>2</sub>RR. In this context, the incorporation of main group metals has been pivotal in optimizing catalytic performance for the production of C<sub>1</sub> and C<sub>2</sub> compounds. When incorporated into copper catalysts, these elements can induce lattice strain, alter the electronic density of states, and create new active sites. For instance, some main group metals like Bi can highly inhibit the

competing HER, and thus greatly enhance CO<sub>2</sub> reduction, while Al doping can introduce electron-deficient regions near the copper surface, enhancing the adsorption of CO<sub>2</sub> and facilitating its activation. This, in turn, can lead to improved CO<sub>2</sub> reduction efficiency and selectivity towards desired products. Additionally, the presence of main-group metals can stabilize the copper nanostructures, preventing aggregation and enhancing their long-term stability during electrocatalytic reactions.<sup>136</sup>

The introduction of main-group elements can enhance the control of copper-based catalysts over the electrochemical CO<sub>2</sub>RR for selective generation of C<sub>1</sub> products. For example, Pan *et al.* electrochemically deposited the main group metal indium (In) onto CuCl-decorated copper foil, successfully constructing a Cu–CuInO<sub>2</sub> dual-metal material with a stable Cu<sup>0</sup>/Cu<sup>+</sup> state. It was found that the high HER overpotential of In could minimize parasitic H<sub>2</sub> production, directing more electrons to CO<sub>2</sub> reduction, which enabled CuInO<sub>2</sub> catalysts to achieve FE<sub>HER</sub> < 15% and FE<sub>CO</sub> of 89% at –0.9 V vs. RHE. The CuInO<sub>2</sub> catalyst demonstrated unique synergistic effects through electronic structure modulation, wherein p-orbitals of In hybridize with d-orbitals of Cu to redistribute charge density, optimize \*CO binding energy, weaken \*CO adsorption, and strengthen \*COOH stabilization, thereby favoring CO production over C<sub>2</sub> pathways (Fig. 9a).<sup>137</sup> Numerous investigations have demonstrated that incorporating main group elements into copper-based catalysts can substantially enhance the catalytic pathway by lowering the energy barrier for C–C coupling, thereby promoting the formation of C<sub>2</sub> products. For example, Wang, Jiang *et al.* reported the construction of a CuO/SnO<sub>2</sub> dual-metal heterostructure through *in situ* electrochemical evolution, successfully regulating the C<sub>1</sub>/C<sub>2</sub> product selectivity through the introduction of Sn. Most importantly, Sn<sup>2+</sup>/Sn<sup>0</sup> in Cu/SnO<sub>2–x</sub> (oxygen-deficient SnO<sub>2</sub>) can stabilize \*COOH and \*CHOCO intermediates, thereby facilitating C–C coupling for CH<sub>3</sub>CH<sub>2</sub>OH production. Through strong d-p orbital hybridization between Cu (3d) and SnO<sub>2–x</sub> (O2p), key intermediates are synergistically stabilized, leading to a lowered energy barrier for C<sub>2</sub> product formation. Besides, the introduction of Sn promoted the synergistic adsorption of \*COOH and \*CHOCO intermediates at the Cu/SnO<sub>2–x</sub> interface, significantly enhancing ethanol production efficiency (Fig. 9b).<sup>138</sup> Meanwhile, Zhang's group introduced the main group metal Bi to prepare a single-atom Bi-modified Cu alloy (BiCu-SAA) for the first time. The high HER overpotential of Bi effectively suppresses competing reactions, while single-atom Bi doping modulates the electronic structure of Cu to stabilize \*CO intermediates and facilitate efficient C–C coupling. Through this synergistic Bi–Cu interaction, the BiCu-SAA catalyst achieves exceptional performance at industrial current densities (400 mA cm<sup>–2</sup>), delivering a remarkable 73.4% FE for C<sub>2+</sub> products (Fig. 9c and d).<sup>139</sup> In another study, Wang *et al.* incorporated the main-group metal gallium (Ga) into a catalyst system, creating a dual-metal catalyst by combining it with copper (Cu). The resulting CuGa catalyst demonstrated a cathodic energy efficiency (EE) exceeding 50% for C<sub>2+</sub> products at a current density of 1 A cm<sup>–2</sup>, significantly surpassing the performance of pure Cu, which exhibited an EE of



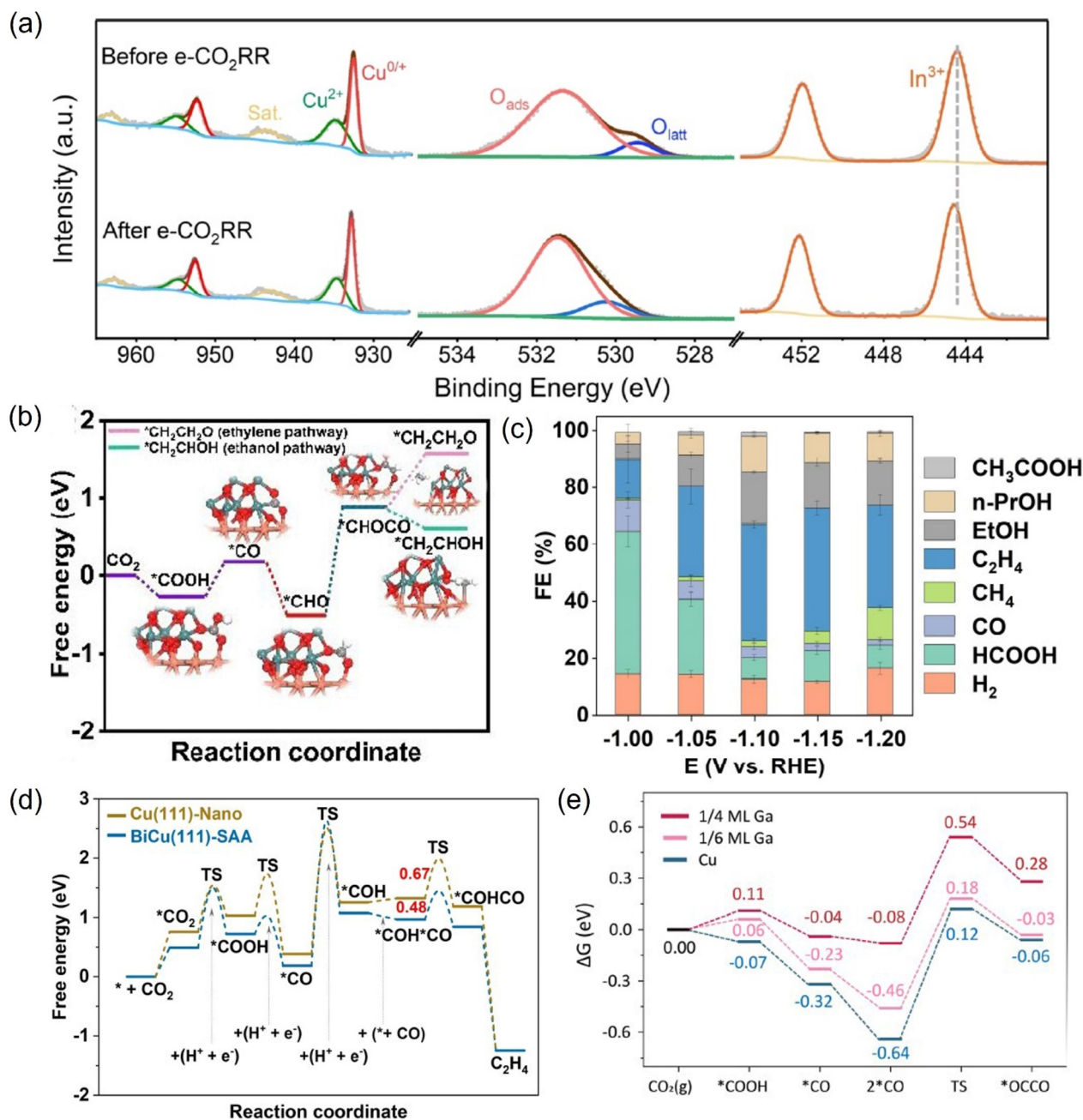


Fig. 9 (a) XPS spectra of Cu-In-120 s before and after the e-CO<sub>2</sub>RR. (b) The comparison of free energy for the ethylene and ethanol pathways on Cu/SnO<sub>2-x</sub>. (c) FE values of various products on the BiCu-SAA at different applied potentials in an H-type cell. (d) The free energy diagram for the CO<sub>2</sub>RR to C<sub>2</sub>H<sub>4</sub> on the BiCu(111)-SAA and Cu(111)-Nano. (e) The free energy surface for CO<sub>2</sub> reduction to CO and CO-CO coupling with the Cu (100) surface with 0, 1/6, and 1/4 ML of Ga. (a) Reproduced with permission.<sup>137</sup> Copyright 2023, American Chemical Society. (b) Reproduced with permission.<sup>138</sup> Copyright 2023, John Wiley and Sons Ltd. (c and d) Reproduced with permission.<sup>139</sup> Copyright, 2023, John Wiley and Sons Ltd. (e) Reproduced with permission.<sup>140</sup> Copyright 2024, Springer Nature.

approximately 30%. They discovered that Ga, with its lower electronegativity than Cu, can donate electrons to Cu, increasing the occupancy of Cu's sp-band, which strengthened  $\sigma$ -repulsion between Cu and adsorbed CO (\*CO), weakening \*CO binding energy. Besides, Ga can stabilize Cu<sup>+</sup> states under ambient conditions, which may facilitate \*CO adsorption and C-C coupling, leading to the high performance for C<sub>2</sub><sup>+</sup> production (Fig. 9e).<sup>140</sup>

In summary, the incorporation of main-group metals into copper-based catalysts offers a powerful strategy to optimize CO<sub>2</sub> electroreduction by modulating electronic and geometric properties. These elements enhance selectivity and efficiency—either by suppressing the HER, stabilizing key intermediates, or lowering C-C coupling barriers—enabling high-performance C<sub>1</sub> or C<sub>2</sub><sup>+</sup> production.

**3.2.2 Copper and non-precious transition metals.** Non-precious transition metals, such as iron (Fe), cobalt (Co), nickel (Ni), and zinc (Zn) are attractive dopants for copper-based nanomaterials due to their abundance, low cost, and potential to enhance catalytic activity. These metals can form alloys or intermetallic compounds with copper, leading to synergistic effects that improve CO<sub>2</sub> adsorption and reduction kinetics. The d-electron configuration of transition metals plays a crucial role in determining their catalytic properties. When a non-noble transition metal atom, such as Co, substitutes a copper atom in a Cu-based catalyst, it induces a drastic change in the density of states (DOS).<sup>141</sup> Moreover, when a non-noble transition metal with a different electronegativity is introduced into the copper lattice, it can lead to bond polarization. This polarization affects the distribution of electron density around the active sites, influencing the adsorption and activation of CO<sub>2</sub> molecules.<sup>142</sup> The d-electron interactions and electronegativity differences between the dopant atoms and copper play crucial roles in determining the catalytic pathway and efficiency for the CO<sub>2</sub>RR. Furthermore, the presence of non-precious transition metals can modulate the surface energy and reactivity of copper, enabling the tuning of product selectivity and reaction rates.<sup>143</sup>

Many previous studies have shown that non-precious transition metals, owing to their distinctive d-electron configurations, can modulate the electronic structure and surface properties of Cu catalysts. Streb *et al.* developed a CuCo dual-metal electrocatalyst, formed under reaction conditions that drive Cu sites from single-atom states into small Cu clusters (Cu<sup>0</sup>) while maintaining Co sites in a monodispersed state, which enabled highly selective CO<sub>2</sub>-to-EtOH conversion with a FE > 70%. It was discovered that a synergistic CO spillover mechanism occurred where Co sites efficiently generated CO and created a high local CO concentration, while Cu sites received this CO and facilitate C–C coupling to produce EtOH, thereby significantly enhancing C<sub>2</sub> product selectivity by reducing the CO transport distance. The close proximity of Co and Cu sites enables efficient CO<sub>2</sub>-to-ethanol conversion through the CO spillover mechanism, while inhibiting side reactions, demonstrating the importance of dual-metal catalysts in designing efficient CO<sub>2</sub> reduction systems (Fig. 10a).<sup>59</sup> In another study, Ma, Zhang, *et al.* added a trace amount of Ni to the surface of CuO nanosheets which markedly improved both the stability and FE for the electrochemical reduction of CO<sub>2</sub> into C<sub>2</sub> products. Ni doping into CuO nanosheets could significantly inhibit the dissolution of Cu during the CO<sub>2</sub>RR by strengthening the bonds between surface and subsurface Cu atoms. Hence, unlike pure CuO, which is prone to transforming into dendritic structures during prolonged reactions, the CuO + Ni-surface dual-metal system maintains its nanosheet architecture, ensuring consistent and reliable catalytic performance over time. DFT calculations and *operando* ATR-SEIRAS revealed that Ni-doped CuO surfaces exhibited stronger \*CO adsorption and lower energy barriers for \*CO dimerization, promoting C–C coupling, offering a cost-effective synergistic strategy to enhance CO<sub>2</sub>RR efficiency and durability for C<sub>2</sub> production (Fig. 10b and c).<sup>62</sup> The non-precious transition metal Zn is rich

with d electrons. Schuhmann *et al.* doped the Cu-based catalyst with Zn to obtain the dual-metal gas diffusion electrodes (GDEs) B–Cu–Zn, which can enhance the electrocatalytic CO<sub>2</sub>RR activity toward multi-carbon C<sub>2+</sub> products with high stability. *Operando* Raman spectroscopy confirmed that Zn incorporation helps retain Cu<sup>+</sup> species under reduction conditions, which can suppress the HER and facilitate C–C coupling, while the Cu<sup>+</sup> sites could lower the energy barrier for \*OCCO intermediate formation, the key step in C<sub>2+</sub> production. The synergistic interplay between Cu and Zn in B–Cu–Zn GDEs significantly improved the CO<sub>2</sub>RR performance mainly through the stabilization of Cu<sup>+</sup> species by Zn and dynamic protection of active site Cu through Zn sacrificial oxidation (Fig. 10d and e).<sup>60</sup>

In summary, the incorporation of non-precious transition metals into Cu-based catalysts introduces synergistic effects that significantly enhance CO<sub>2</sub> electroreduction toward C<sub>2+</sub> products. These dopants modify the electronic structure of Cu through their distinct d-electron configurations and electronegativity differences, optimizing CO<sub>2</sub> adsorption, stabilizing key intermediates like \*CO and \*OCCO, and lowering energy barriers for C–C coupling. Studies on CuCo, CuNi, and CuZn nanoparticle systems demonstrate that dual-metal interactions—such as CO spillover, strengthened Cu surface bonding, and sacrificial stabilization of Cu<sup>+</sup>—play pivotal roles in improving selectivity and durability at high current densities.<sup>61</sup> These findings highlight the potential of cost-effective dual-metal catalysts to advance the CO<sub>2</sub>RR by precisely tuning electronic and geometric properties, offering a scalable pathway for sustainable C<sub>2+</sub> production.

**3.2.3 Copper and precious transition metals.** Noble metals, such as silver (Ag), gold (Au), and palladium (Pd), are well-known for their exceptional catalytic properties and are often used as dopants to enhance the performance of copper-based nanomaterials in CO<sub>2</sub> reduction. These metals can act as co-catalysts, promoting the activation of CO<sub>2</sub> and facilitating the formation of key reaction intermediates. For instance, Ag doping has been reported to increase the FE of copper-based catalysts towards ethylene production, owing to the ability of Ag to stabilize the \*CO intermediate and promote its subsequent dimerization.<sup>144</sup> Similarly, Au doping can enhance the selectivity towards multi-carbon products by modulating the adsorption energy of reaction intermediates on the copper surface. However, the high cost of noble metals necessitates the development of strategies for their efficient utilization and recycling.<sup>145</sup>

Compared to other noble metals like Au, Pd, and Pt for doping Cu-based CO<sub>2</sub>RR catalysts, Ag presents distinct and superior advantages, particularly in terms of cost-effectiveness. Moreover, Ag demonstrates weaker \*CO adsorption compared to Cu but stronger adsorption than Au, thereby establishing an optimal intermediate state conducive to C–C coupling. For example, Wang, Ye, *et al.* developed a Ag-doped Cu<sub>2</sub>O–Cu catalyst, Ag/Cu<sub>2</sub>O–Cu, which can significantly enhance CO<sub>2</sub> electroreduction CO<sub>2</sub> to multi-carbon C<sub>2+</sub> products at an industrial current density of 1.0 A cm<sup>−2</sup> with a FE of 76.5%. *Operando* Raman spectroscopy and XPS analyses confirmed that Ag incorporation effectively stabilizes metastable Cu<sup>+</sup> species





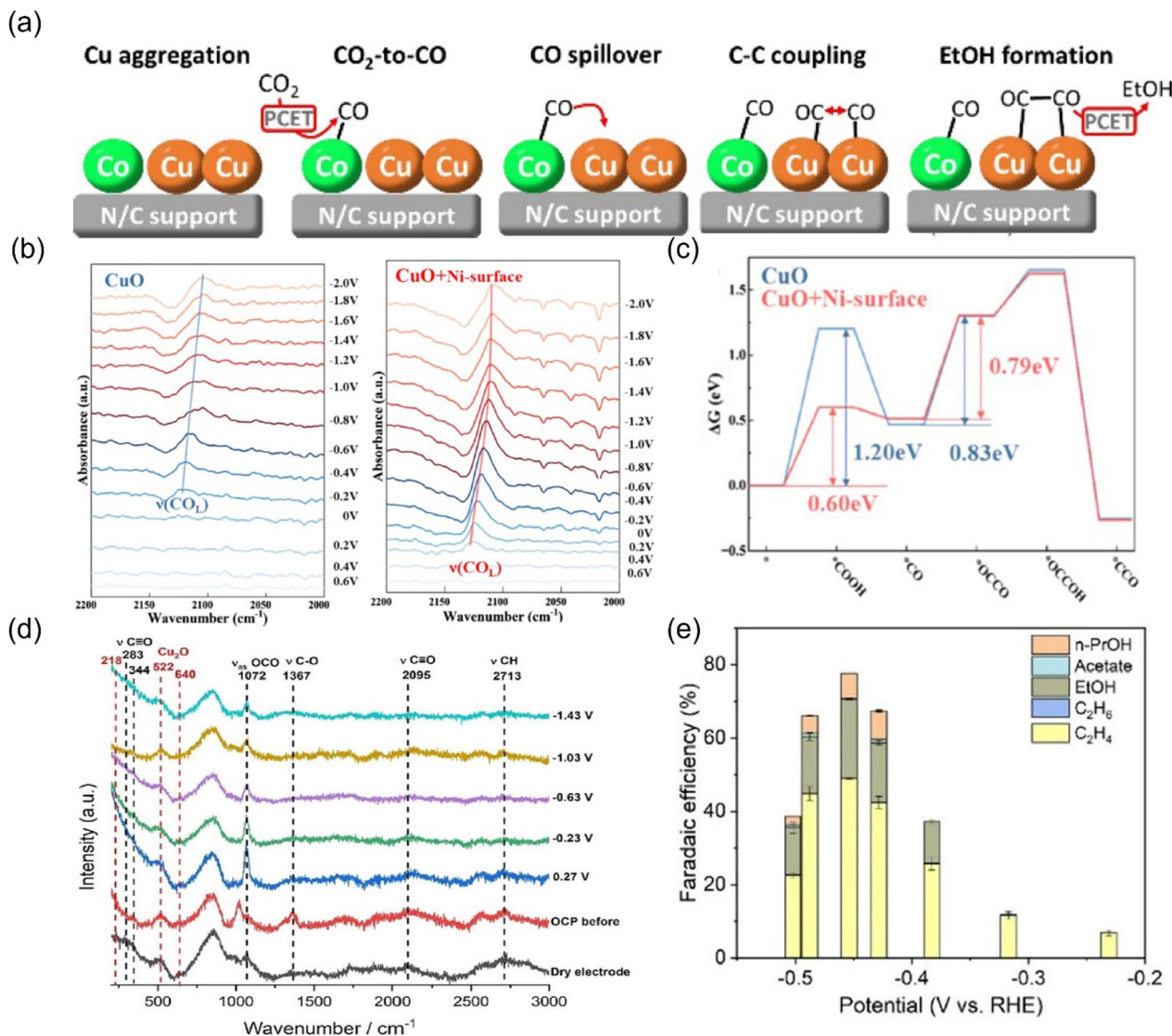
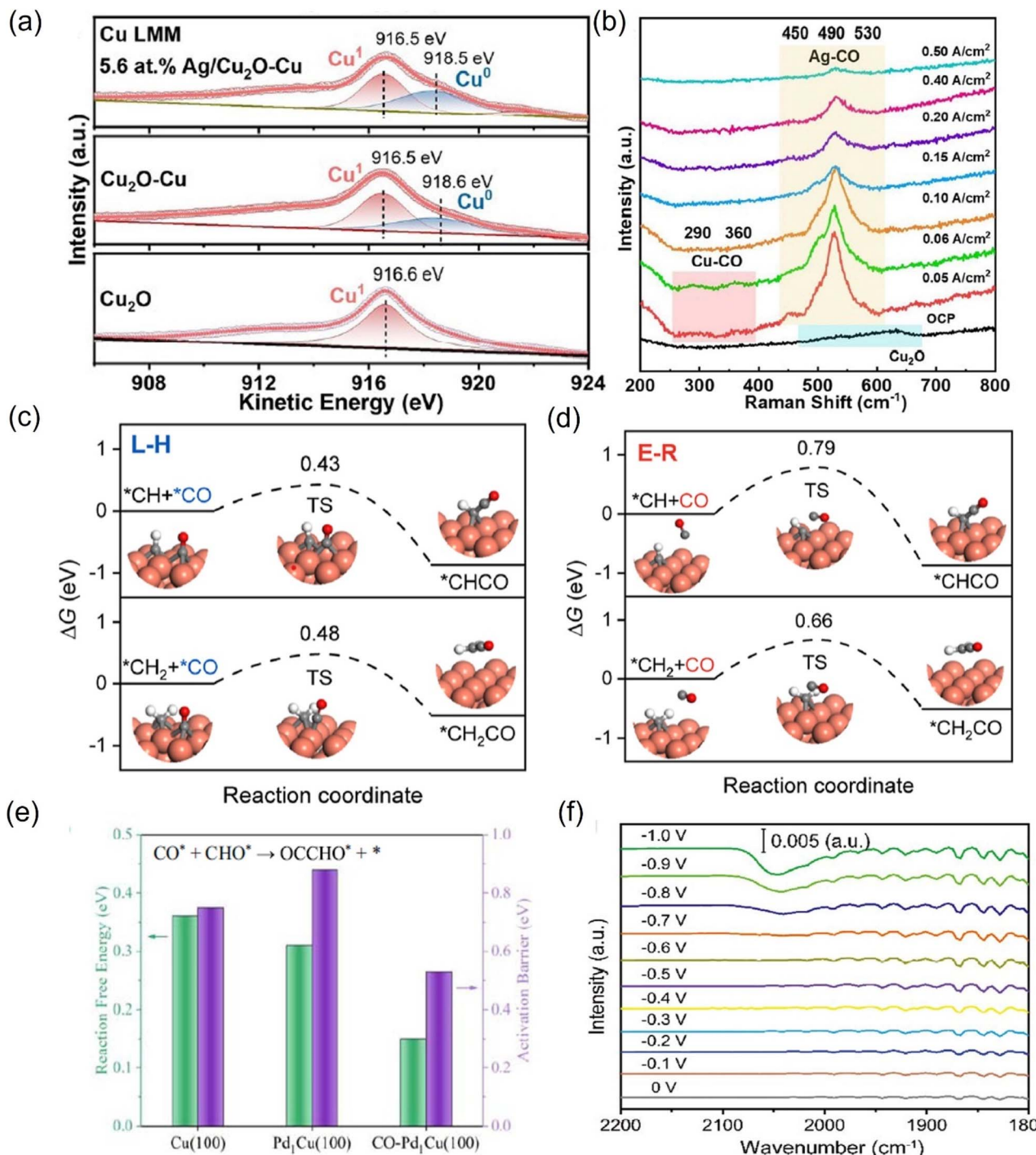


Fig. 10 (a) The CO spillover mechanism for efficient ethanol formation at the CoCu electrocatalyst. (b) FT-IR characterization of CuO and the CuO + Ni-surface. (c) Relative Gibbs free energy diagrams for the CO<sub>2</sub>RR. (d) *Operando* electrochemical Raman spectra for the 0.5B-Cu : 0.025Zn GDE. (e) Faradaic efficiencies for CO<sub>2</sub>RR products at a catalyst loading of 0.5 mg cm<sup>-2</sup> B-Cu at different potentials. (a) Reproduced with permission.<sup>59</sup> Copyright 2024, American Chemical Society. (b and c) Reproduced with permission.<sup>62</sup> Copyright 2025, Elsevier. (d and e) Reproduced with permission.<sup>60</sup> Copyright 2021, John Wiley and Sons Ltd.

(Cu<sub>2</sub>O) under reducing conditions, maintaining robust Ag/Cu<sup>+</sup>/Cu<sup>0</sup> interfaces during the CO<sub>2</sub>RR, which is a critical feature for facilitating C-C coupling. The intermediate \*CO binding strength of Ag (between Cu and Au) creates a synergistic system, where efficient \*CO production couples with facile spillover to Cu<sup>+</sup>/Cu<sup>0</sup> sites, lowering the \*OCCO formation barrier by 56% *versus* Cu<sub>2</sub>O and dramatically boosting C<sub>2</sub><sup>+</sup> selectivity (Fig. 11a and b).<sup>144</sup> Li's research group also developed a Ag-doped Cu-based material featuring (111)-facet-exposed Cu nanosheets decorated with Ag nanoparticles. This composite demonstrated remarkable efficiency in electrochemically converting CO<sub>2</sub> to ethanol, achieving a FE of 56.5 ± 2.6% and a partial current density of 356.7 ± 9.5 mA cm<sup>-2</sup>. They discovered that the synergistic effect between Ag and Cu in the dual-metal catalyst lies in Ag's ability to supply CO to Cu(111) facets—which

efficiently generate \*CH<sub>2</sub> intermediates—promoting asymmetric \*CH<sub>2</sub>-CO coupling for ethanol production, while suppressing excessive \*CO hydrogenation to methane (FE drops from 27.3% on bare Cu to 3.7%) and shifting selectivity away from symmetric CO-CO coupling that favors ethanol production. This dynamic interplay, enhanced by the layered Cu/Ag structure, optimizes local CO coverage and intermediate utilization, steering selectivity toward ethanol over hydrocarbons (Fig. 11c and d).<sup>146</sup>

Many significant studies have highlighted the promotional role of doping other precious metals, such as Pd and Au, into Cu-based nanomaterials in facilitating the electrocatalytic reduction of CO<sub>2</sub>. For example, Yang, Che, *et al.* reported two platinum-group-metal doped Cu-based dual-metal catalysts Pd<sub>1</sub>Cu and Pt<sub>1</sub>Cu for the electrocatalytic CO<sub>2</sub>RR. It was found



**Fig. 11** (a) Cu LMM spectra of Cu<sub>2</sub>O, Cu<sub>2</sub>O-Cu, and 5.6 atom% Ag/Cu<sub>2</sub>O-Cu catalysts. (b) Raman shift of the 5.6 atom% Ag/Cu<sub>2</sub>O-Cu catalyst. DFT calculations: barriers for \*CH<sub>x</sub> (x = 1, 2) coupling with \*CO/CO via (c) L-H and (d) E-R mechanisms. (e) The reaction free energies and activation barriers of C-C coupling on Cu (100) and Pd<sub>1</sub>Cu (100). (f) *In situ* ATR-IR spectra of Au-Cu Janus NSs. (a and b) Reproduced with permission.<sup>144</sup> Copyright 2025, American Chemical Society. (c and d) Reproduced with permission.<sup>146</sup> Copyright 2024, American Chemical Society. (e) Reproduced with permission.<sup>147</sup> Copyright 2023, Springer Nature. (f) Reproduced with permission.<sup>148</sup> Copyright 2022, Wiley-VCH Verlag.

that both Pt and Pd single-atom dopants boost CO\* adsorption on Cu, serving as CO\* reservoirs that balance coverage and prevent poisoning, thereby enhancing C-C coupling for hydrocarbon production. In addition, Pt and Pd single-atom doping

in Cu synergistically enhances the CO<sub>2</sub>RR by enriching CO\* coverage while suppressing the HER and preserving facet-dependent selectivity (CH<sub>4</sub> on Cu (111) and C<sub>2</sub>H<sub>4</sub> on Cu (100)). Meanwhile, Pd<sub>1</sub>Cu demonstrates superior performance (CH<sub>4</sub>:

25%; C<sub>2</sub>H<sub>4</sub>: 33%) by optimally balancing CO\* stabilization and hydrogenation kinetics compared to Pt<sub>1</sub>Cu (Fig. 11e).<sup>147</sup> Huang *et al.* reported gold-copper (Au-Cu) Janus nanostructures as a dual-metal catalyst capable of efficiently electroreducing CO<sub>2</sub> to C<sub>2+</sub> products, achieving a C<sub>2+</sub> selectivity of 67%. *In situ* ATR-IR spectroscopy revealed that the Au-Cu synergy enables selective CO<sub>2</sub>-to-CO\* conversion at Au sites (the critical intermediate for C-C coupling) *via* weak CO\* binding, while adjacent Cu sites facilitate CO\* hydrogenation to hydrocarbons and C-C coupling. The enhanced CO\* coverage on Au-Cu Janus nanostructures compared to pure Cu can be attributed to CO\* spillover from Au to Cu domains. They discovered that fine-tuning Au-Cu interfaces of Janus structures could enhance selectivity toward C<sub>2+</sub> products, which outperformed the physical mixtures or core-shell structures in the CO<sub>2</sub>RR, offering a general strategy for multi-step reaction catalysts (Fig. 11f).<sup>148</sup>

In summary, doping noble metals like Ag, Pd, and Au into Cu-based nanomaterials significantly enhances their performance in CO<sub>2</sub> electroreduction.<sup>149</sup> Ag stands out for its cost-effectiveness and optimal CO adsorption strength, facilitating C-C coupling and boosting C<sub>2+</sub> selectivity. Pd and Au doping also promote CO adsorption and balance coverage, preventing poisoning and enhancing C-C coupling for hydrocarbon production.<sup>150</sup> These findings underscore the critical role of precious transition metal doped Cu-based dual-metal synergies in modulating intermediate adsorption energies, stabilizing reactive species, and steering selectivity toward high-value C<sub>2+</sub> products.

**3.2.4 Copper and lanthanide metals.** Lanthanide metal elements, such as cerium (Ce), lanthanum (La), gadolinium (Gd) and neodymium (Nd) possess unique electronic properties that can be harnessed to enhance the performance of copper-based nanomaterials in CO<sub>2</sub> reduction.<sup>151,152</sup> The unique f-orbital electrons of lanthanide metal elements significantly influence their doping effects in copper-based nanomaterials for electrocatalytic CO<sub>2</sub> reduction.<sup>135,153</sup>

The incorporation of lanthanides into copper-based catalysts introduces lattice strain due to the substantial difference in ionic radii between lanthanides and copper.<sup>149,154,155</sup> This strain can modulate the electronic structure and binding energies of reaction intermediates, thereby lowering the activation energy barriers and optimizing the reaction pathway for CO<sub>2</sub> reduction.<sup>156</sup> Han, Sun, *et al.* reported that the atomic doping of Gd into CuO<sub>x</sub> catalysts (Gd<sub>1</sub>/CuO<sub>x</sub>) induces tensile strain and stabilizes Cu<sup>+</sup> species, enabling an exceptional FE of 81.4% for C<sub>2+</sub> products with a partial current density of 444.3 mA cm<sup>-2</sup> at -0.8 V *vs.* RHE, demonstrating its high efficiency in the CO<sub>2</sub>RR. They discovered that the unique 4f electron configuration and unfilled 5d orbitals of Gd can enhance spin-orbit coupling, modifying the local electron density around Cu atoms and inhibiting their reduction to Cu<sup>0</sup>. This Gd-Cu synergy facilitated efficient electron transfer during the CO<sub>2</sub>RR, significantly improving reaction kinetics. Additionally, the tensile strain induced through the large ionic radius of Gd introduced into the CuO<sub>x</sub> lattice could optimize the d-band center of Cu and fine-tune the binding energy of key intermediates \*CO. This strain effect further reduces the Gibbs free energy barrier for the

C-C coupling step (2CO → O\*CCO), thereby promoting the selective formation of C<sub>2+</sub> products (Fig. 12a and b).<sup>157</sup> Liang *et al.* constructed a Cu/CeO<sub>2</sub> dual-metal catalyst, in which the larger lattice spacing of the CeO<sub>2</sub> (111) plane compared to Cu<sub>2</sub>O stretches Cu-O bonds, introducing tensile strain in the Cu domains. It was discovered that the tensile strain in the Cu/CeO<sub>2</sub> heterostructure upshifted the d-band center of Cu, which can enhance \*CO adsorption and promote dimerization, facilitating C-C coupling for multicarbon formation. DFT calculations revealed that the synergistic Cu and CeO<sub>2</sub> interaction drives charge transfer from Cu to CeO<sub>2</sub>, creating electron-deficient interfacial Cu sites. By combining tensile strain and electron deficiency, Cu and CeO<sub>2</sub> synergistically optimize CO coverage and stabilize key intermediates, collectively boosting selectivity toward C<sub>2+</sub> products (Fig. 12c and d).<sup>158</sup>

Additionally, the unique electronic configurations of lanthanides can also regulate the electronic structure of active sites or modulate the d-band center of copper, enhancing \*CO adsorption and stabilizing Cu<sup>+</sup> sites critical for multicarbon product formation. Han, Zhu, *et al.* developed a Pr-Cu dual-metal oxide heterointerface, specifically Pr<sub>6</sub>O<sub>11</sub>-Cu-SS, which efficiently catalyzes the CO<sub>2</sub>RR to C<sub>2+</sub> products, achieving a high FE of 71.3% for C<sub>2+</sub> alcohols (ethanol and *n*-propanol) at a current density of 700 mA cm<sup>-2</sup>. It was found that Pr doping in Cu oxides could generate an oxygen vacancy (O<sub>vac</sub>)-rich interface, which modulated the electronic structure of Cu (Cu<sup>δ+</sup>/Cu<sup>0</sup>) to enhance CO adsorption and asymmetric C-C coupling. The Pr-O-Cu linkages further stabilized key intermediates, enabling sustained high activity and stability even at industrial current densities. DFT calculations and *in situ* Raman spectroscopy revealed that the Pr-Cu interface induced mixed \*CO adsorption configurations, in which this asymmetry promoted C<sub>2+</sub> alcohol formation over ethylene by stabilizing \*OCHCH<sub>3</sub> intermediates (Fig. 12e).<sup>159</sup> In another study, Han, Sun, *et al.* developed a La-doped Cu electrocatalyst that achieved a remarkable FE of 86.2% for C<sub>2+</sub> products at a partial current density of -775.8 mA cm<sup>-2</sup> in acidic electrolyte during CO<sub>2</sub> reduction. As validated by *in situ* SERS detection, owing to the synergistic effects of La and Cu, the mesoporous channels in La-Cu hollow spheres (La-Cu HS) could concentrate K<sup>+</sup> and OH<sup>-</sup> near the catalyst surface, creating a localized alkaline microenvironment that can suppress the HER and promote C-C coupling. Electronic structure analysis reveals that due to the difference in electronegativity, La can donate electrons to Cu, which enhances \*CO stabilization. DFT calculations further confirm that the resulting La-O-Cu linkages could stabilize metallic Cu during the CO<sub>2</sub>RR, while enabling synergistic catalysis, where La promoted CO generation and lowered C-C coupling barriers, while Cu maintained conductive pathways and active sites for CO<sub>2</sub> reduction.<sup>160</sup>

In summary, the integration of lanthanide metals into copper-based nanomaterials presents a promising strategy for enhancing CO<sub>2</sub> reduction performance. By leveraging the unique electronic properties of lanthanides, such as their f-orbital electrons and specific electron configurations, researchers have been able to modulate the reaction pathways of copper-based catalysts.<sup>158</sup> The synergistic interactions between copper and lanthanides, driven by factors such as





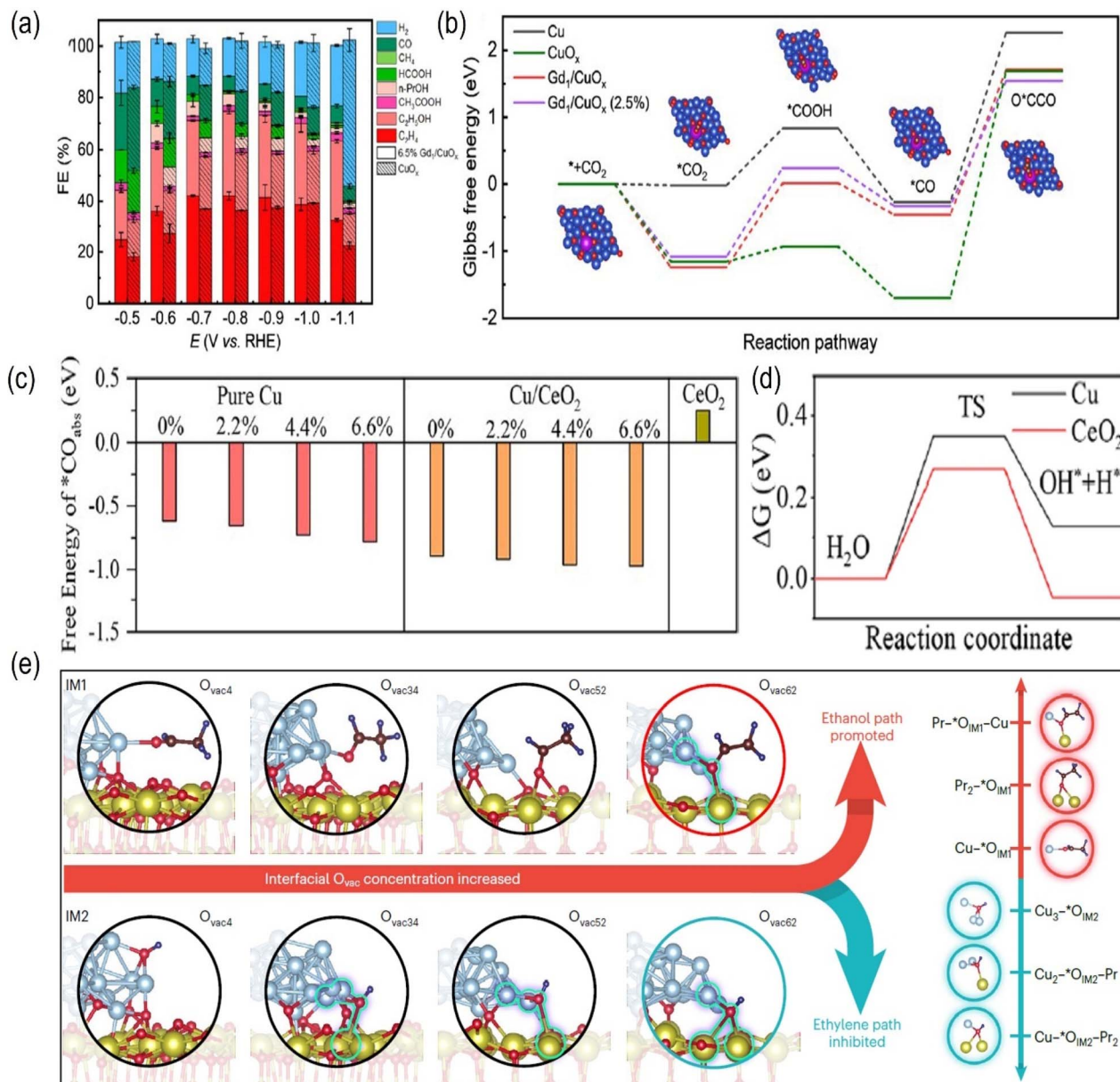


Fig. 12 (a) Faradaic efficiencies for CO<sub>2</sub>RR products on 6.5% Gd<sub>1</sub>/CuO<sub>x</sub> and CuO<sub>x</sub>. (b) The free energy diagram of the CO<sub>2</sub>RR for Cu, CuO<sub>x</sub>, Gd<sub>1</sub>/CuO<sub>x</sub>, and Gd<sub>1</sub>/CuO<sub>x</sub> (2.5%). (c) Calculated \*CO adsorption energies on standard Cu, stretched Cu, Cu/CeO<sub>2</sub>, the stretched Cu/CeO<sub>2</sub> interface, and CeO<sub>2</sub>. (d) The transition barrier investigation for H<sub>2</sub>O dissociation on Cu (111) and CeO<sub>2</sub> (111). (e) Adsorption configurations of different Pr<sub>6</sub>O<sub>11</sub>-O<sub>vac</sub>-Cu models. (a and b) Reproduced with permission.<sup>157</sup> Copyright 2023, American Chemical Society. (c and d) Reproduced with permission.<sup>158</sup> Copyright 2023, American Chemical Society. (e) Reproduced with permission.<sup>159</sup> Copyright, 2025, Springer Nature.

lattice strain, electron transfer, and interface engineering, have opened up new avenues for the development of highly efficient electrocatalysts for the CO<sub>2</sub>RR.<sup>161</sup>

## 4 Conclusions

The development of dual-metal synergistic catalysts has emerged as a powerful strategy to enhance the efficiency, selectivity, and stability of the electrocatalytic CO<sub>2</sub>RR. This review systematically explores the design principles, mechanistic insights, and catalytic performance of dual-metal catalysts, emphasizing the

critical role of synergistic effects of different metal centers in optimizing CO<sub>2</sub>RR pathways, and elucidating the structure-activity correlations. Leveraging the unique synergistic effects of two metal centers has led to remarkable progress in tailoring catalyst properties to favor desired reaction intermediates and suppress competing HER.

This review first focuses the design principles of dual-metal catalysts with synergistic effects for the CO<sub>2</sub>RR, focusing on electronic and geometric structure regulation. Electronic structure regulation involves chemical state, vacancy, and coordination environment modifications, while geometric structure regulation

encompasses crystal facet, nanoparticle size, and morphology adjustments. These strategies are crucial for optimizing the adsorption and activation of reactants, stabilizing intermediate states, and refining the catalytic pathway. Next, the review delves into the influence of different types of dual-metal active sites, including dual-atom metal catalysts (DACs) and dual-metal nanomaterial catalysts. DACs are characterized by their atomic efficiency and precise electronic structures, while dual-metal nanomaterial catalysts offer more complex surface architectures and synergistic effects at the nanoscale. For dual-metal nanomaterial catalysts, various secondary metals, such as main-group metals, non-precious transition metals, noble metals and lanthanides, are studied for their potential to enhance copper-based catalysts for CO<sub>2</sub>RR performance. The review mainly explores various dual-metal catalysts with synergistic catalytic effects, highlighting their distinct advantages and mechanisms for promoting the CO<sub>2</sub>RR. The review also underscores the importance of rational design and innovative synthesis strategies in developing advanced CO<sub>2</sub>RR electrocatalysts.

Despite the significant progress made in dual-metal catalysis for the CO<sub>2</sub>RR, several challenges remain. Future research should focus on the following areas: (1) enhanced catalytic stability: improving the long-term stability of dual-metal catalysts is crucial for their practical application. Strategies such as surface passivation, defect engineering, and support optimization could be explored to mitigate deactivation pathways. (2) Developing scalable and cost-effective production methods for dual-metal catalysts is essential for their commercialization. Research on continuous flow reactors, high-throughput screening, and catalyst recycling could accelerate this process. (3) Deeper understanding of the synergistic mechanisms in dual-metal catalysts is needed to guide the rational design of more efficient catalysts. Advanced characterization techniques, such as *operando* spectroscopy and *in situ* electron microscopy, could provide valuable insights. (4) Achieving high selectivity towards multi-carbon products remains a challenge. The optimization of catalyst composition, structure and reaction conditions could pave the way for the efficient production of C<sub>2+</sub> compounds from the CO<sub>2</sub>RR.

In summary, dual-metal catalysis with synergistic effects holds great promise for advancing the field of the CO<sub>2</sub>RR. With continued research efforts in catalyst design, synthesis, and mechanistic understanding, the efficient conversion of CO<sub>2</sub> into value-added products could become a reality, contributing significantly to global carbon neutrality goals.

## Data availability

No primary research results, software or code have been included and no new data were generated or analysed as part of this review.

## Author contributions

M. W. and T. L. conceived the topic and revised the review. M. W., P. S. and Y. Y wrote and edited the original draft of the manuscript. All authors helped in literature search.

## Conflicts of interest

The authors declare no conflict of interest.

## Acknowledgements

This work was supported by the National Natural Science Foundation of China (22375148) and the National Key R&D Program of China (2022YFA1502902).

## Notes and references

- 1 A. Husile, Z. Wang and J. Guan, *Chem. Sci.*, 2025, **16**, 5413–5446.
- 2 D. Suri, S. Das, S. Choudhary, G. Venkanna, B. Sharma, M. A. Afroz, N. K. Tailor, R. Joshi, S. Satapathi and K. Tripathi, *Small*, 2025, **21**, 2408981.
- 3 S. A. Montzka, E. J. Dlugokencky and J. H. Butler, *Nature*, 2011, **476**, 43–50.
- 4 H. M. A. Sharif, M. Rashad, I. Hussain, A. Abbas, O. F. Aldosari and C. Li, *Appl. Catal. B Environ. Energy*, 2024, **344**, 123585.
- 5 W. Lai, Z. Ma, J. Zhang, Y. Yuan, Y. Qiao and H. Huang, *Adv. Funct. Mater.*, 2022, **32**, 2111193.
- 6 M. J. Gidden, T. Gasser, G. Grassi, N. Forsell, I. Janssens, W. F. Lamb, J. Minx, Z. Nicholls, J. Steinhäuser and K. Riahi, *Nature*, 2023, **624**, 102–108.
- 7 B. Buchner, *Science*, 2024, **386**, 601.
- 8 L. Wang, D. Wang and Y. Li, *Carbon Energy*, 2022, **4**, 1021–1079.
- 9 W. Peng, F. Li, S. Kong, C. Guo, H. Wu, J. Wang, Y. Shen, X. Meng and M. Zhang, *Carbon Energy*, 2024, **6**, e498.
- 10 J. Han, X. Bai, X. Xu, X. Bai, A. Husile, S. Zhang, L. Qi and J. Guan, *Chem. Sci.*, 2024, **15**, 7870–7907.
- 11 Z. Wang, Z. Sun, H. Yin, H. Wei, Z. Peng, Y. X. Pang, G. Jia, H. Zhao, C. H. Pang and Z. Yin, *eScience*, 2023, **3**, 100136.
- 12 Y. Yang, S. Louisia, S. Yu, J. Jin, I. Roh, C. Chen, M. V. Fonseca Guzman, J. Feijóo, P.-C. Chen, H. Wang, C. J. Pollock, X. Huang, Y.-T. Shao, C. Wang, D. A. Muller, H. D. Abruña and P. Yang, *Nature*, 2023, **614**, 262–269.
- 13 N. Dutta and S. C. Peter, *J. Am. Chem. Soc.*, 2025, **147**, 9019–9036.
- 14 G. Liang, S. Yang, C. Wu, Y. Liu, Y. Zhao, L. Huang, S. Zhang, S. Dou, H. Du, D. Cui and L. Lin, *J. Mater. Chem. A*, 2025, **13**, 11210–11235.
- 15 J. Jia, Z. Zhang, A. Wang, Y. Liu, Z. Liu, J. Wang, Y. Guo, L. Peng, J. Li and J. Robertson, *Adv. Funct. Mater.*, 2025, **35**, 2412056.
- 16 W. Lai, Y. Qiao, Y. Wang and H. Huang, *Adv. Mater.*, 2023, **35**, 2306288.
- 17 F. Xie, Z. Wang, C.-W. Kao, J. Lan, Y.-R. Lu and Y. Tan, *Angew. Chem., Int. Ed.*, 2024, **63**, e202407661.
- 18 B. Lei, W. Cui, P. Chen, L. Chen, J. Li and F. Dong, *ACS Catal.*, 2022, **12**, 9670–9678.
- 19 J. Xiong, J. Ji, Q. Lei, X. Yang, Y. Bai, X. Zhang and H.-M. Cheng, *eScience*, 2024, 100306.



- 20 K. Wang, K. Huang, Z. Wang, G. An, M. Zhang, W. Liu, S. Fu, H. Guo, B. Zhang, C. Lian, J. Wu and L. Wang, *Small*, 2025, 2502733.
- 21 Q. Yang, H. Liu, Y. Lin, D. Su, Y. Tang and L. Chen, *Adv. Mater.*, 2024, **36**, 2310912.
- 22 H. Zhao, R. Yu, S. Ma, K. Xu, Y. Chen, K. Jiang, Y. Fang, C. Zhu, X. Liu, Y. Tang, L. Wu, Y. Wu, Q. Jiang, P. He, Z. Liu and L. Tan, *Nat. Catal.*, 2022, **5**, 818–831.
- 23 H. Ou, S. Ning, P. Zhu, S. Chen, A. Han, Q. Kang, Z. Hu, J. Ye, D. Wang and Y. Li, *Angew. Chem., Int. Ed.*, 2022, **61**, e202206579.
- 24 Z. Wu, N. Meng, R. Yang, M. Chen, J. Pan, S. Chi, C. Wu, S. Xi, Y. Liu, Y. Ou, W. Wu, S. Han, B. Zhang, Q.-H. Yang and K. Ping Loh, *Angew. Chem., Int. Ed.*, 2025, **64**, e202420283.
- 25 C.-f. Li, R.-t. Guo, Z.-r. Zhang, T. Wu and W.-g. Pan, *Small*, 2023, **19**, 2207875.
- 26 M. Kuang, B. Li, L. Zhou, Z. Huang, J. Wu, S. Wang and J. Yang, *Angew. Chem., Int. Ed.*, 2025, **64**, e202422357.
- 27 Y.-F. Tang, L.-B. Liu, M. Yu, S. Liu, P.-F. Sui, W. Sun, X.-Z. Fu, J.-L. Luo and S. Liu, *Chem. Soc. Rev.*, 2024, **53**, 9344–9377.
- 28 T. Lu, T. Xu, S. Zhu, J. Li, J. Wang, H. Jin, X. Wang, J.-J. Lv, Z.-J. Wang and S. Wang, *Adv. Mater.*, 2023, **35**, 2310433.
- 29 H. Shang and D. Liu, *Nano Res.*, 2023, **16**, 6477–6506.
- 30 J. Liu, Y. Cai, R. Song, S. Ding, Z. Lyu, Y.-C. Chang, H. Tian, X. Zhang, D. Du, W. Zhu, Y. Zhou and Y. Lin, *Mater. Today*, 2021, **48**, 95–114.
- 31 Y. Zhai, P. Han, Q. Yun, Y. Ge, X. Zhang, Y. Chen and H. Zhang, *eScience*, 2022, **2**, 467–485.
- 32 J. Wang, D. Deng, Q. Wu, M. Liu, Y. Wang, J. Jiang, X. Zheng, H. Zheng, Y. Bai, Y. Chen, X. Xiong and Y. Lei, *ACS Nano*, 2023, **17**, 18688–18705.
- 33 C. Wang, Z. Lv, X. Feng, W. Yang and B. Wang, *Adv. Energy Mater.*, 2024, **14**, 2400160.
- 34 J. Huang, T. Yang, K. Zhao, S. Chen, Q. Huang and Y. Han, *J. Energy Chem.*, 2021, **62**, 71–102.
- 35 P. Sun, S. Liu, X. Zheng, G. Hu, Q. Zhang, X. Liu, G. Zheng and Y. Chen, *Nano Today*, 2024, **55**, 102152.
- 36 P. Li, J. Liu, Y. Wang, X.-D. Zhang, Y. Hou, Y. Zhang, X. Sun, X. Kang, Q. Zhu and B. Han, *J. Am. Chem. Soc.*, 2024, **146**, 26525–26533.
- 37 Q. Zhang, D. Liu, Y. Zhang, Z. Guo, M. Chen, Y. Chen, B. Jin, Y. Song and H. Pan, *J. Energy Chem.*, 2023, **87**, 509–517.
- 38 Y. Li, H. Wang, X. Yang, T. O'Carroll and G. Wu, *Angew. Chem., Int. Ed.*, 2024, **63**, e202317884.
- 39 L. Shi, J. Song, Y. Yang, L. Yang, Z. Dai, L. Yao and W. Jiang, *J. Mater. Chem. A*, 2025, **13**, 2478–2504.
- 40 J. Jiao, Q. Yuan, M. Tan, X. Han, M. Gao, C. Zhang, X. Yang, Z. Shi, Y. Ma, H. Xiao, J. Zhang and T. Lu, *Nat. Commun.*, 2023, **14**, 6164.
- 41 B. Ren, G. Wen, R. Gao, D. Luo, Z. Zhang, W. Qiu, Q. Ma, X. Wang, Y. Cui, L. Ricardez-Sandoval, A. Yu and Z. Chen, *Nat. Commun.*, 2022, **13**, 2486.
- 42 W. Wu, J. Zhu, Y. Tong, S. Xiang and P. Chen, *Nano Res.*, 2024, **17**, 3684–3692.
- 43 A. R. Woldu, A. G. Yohannes, Z. Huang, P. Kennepohl, D. Astruc, L. Hu and X.-C. Huang, *Adv. Mater.*, 2024, **36**, 2414169.
- 44 Y. Gao, B. Liu and D. Wang, *Adv. Mater.*, 2023, **35**, 2209654.
- 45 Y. Yang, W. Zhang, G. Wu, Q. Huang, J. Wen, D. Wang and M. Liu, *Angew. Chem., Int. Ed.*, 2025, e202504423.
- 46 Y. Chen, J. Zhao, X. Pan, L. Li, Z. Yu, X. Wang, T. Ma, S. Lin and J. Lin, *Angew. Chem., Int. Ed.*, 2024, **63**, e202411543.
- 47 J. Feng, L. Zhang, S. Liu, L. Xu, X. Ma, X. Tan, L. Wu, Q. Qian, T. Wu, J. Zhang, X. Sun and B. Han, *Nat. Commun.*, 2023, **14**, 4615.
- 48 J. Li, Y. Chen, B. Yao, W. Yang, X. Cui, H. Liu, S. Dai, S. Xi, Z. Sun, W. Chen, Y. Qin, J. Wang, Q. He, C. Ling, D. Wang and Z. Zhang, *J. Am. Chem. Soc.*, 2024, **146**, 5693–5701.
- 49 J. Liu, P. Li, J. Bi, S. Jia, Y. Wang, X. Kang, X. Sun, Q. Zhu and B. Han, *J. Am. Chem. Soc.*, 2023, **145**, 23037–23047.
- 50 W. Zhu, L. Zhang, S. Liu, A. Li, X. Yuan, C. Hu, G. Zhang, W. Deng, K. Zang, J. Luo, Y. Zhu, M. Gu, Z.-J. Zhao and J. Gong, *Angew. Chem., Int. Ed.*, 2020, **59**, 12664–12668.
- 51 W. Xu, Y. Wang, C. Zhang, X. Ma, J. Wu, Y. Liu, B. Lu, H. Zhang, C. Ming and J. Xiang, *Chem. Eng. J.*, 2023, **461**, 141911.
- 52 R. Cao, S. Yin, Y. Han, J. Zhang, W. Jiang and G. Liu, *Coord. Chem. Rev.*, 2025, **538**, 216722.
- 53 J. Ji, L. Wu, S. Zhou, T. Qiu, Z. Li, L. Wang, L. Zhang, L. Ma, M. Ling, S. Zhou and C. Liang, *Small Methods*, 2022, **6**, 2101511.
- 54 H. Shang, S. K. Wallentine, D. M. Hofmann, Q. Zhu, C. J. Murphy and L. R. Baker, *Chem. Sci.*, 2020, **11**, 12298–12306.
- 55 B. Zhao, F. Chen, C. Cheng, L. Li, C. Liu and B. Zhang, *Adv. Energy Mater.*, 2023, **13**, 2204346.
- 56 M. Jun, J. Kundu, D. H. Kim, M. Kim, D. Kim, K. Lee and S.-I. Choi, *Adv. Mater.*, 2024, **36**, 2313028.
- 57 Z.-Q. Liang, T.-T. Zhuang, A. Seifitokaldani, J. Li, C.-W. Huang, C.-S. Tan, Y. Li, P. De Luna, C. T. Dinh, Y. Hu, Q. Xiao, P.-L. Hsieh, Y. Wang, F. Li, R. Quintero-Bermudez, Y. Zhou, P. Chen, Y. Pang, S.-C. Lo, L.-J. Chen, H. Tan, Z. Xu and S. Zhao, *Nat. Commun.*, 2018, **9**, 3828.
- 58 M. Qi, M. J. Zachman, Y. Li, Y. Zeng, S. Hwang, J. Liang, M. Lyons, Q. Zhao, Y. Mao, Y. Shao, Z. Feng, Z. Wang, Y. Zhao and G. Wu, *Energy Environ. Sci.*, 2025, **18**, 5643–5656.
- 59 S. A. Chala, R. Liu, E. O. Oseghe, S. T. Clausing, C. Kampf, J. Bansmann, A. H. Clark, Y. Zhou, I. Lieberwirth, J. Biskupek, U. Kaiser and C. Streb, *ACS Catal.*, 2024, **14**, 15553–15564.
- 60 Y. Song, J. R. C. Junqueira, N. Sikdar, D. Öhl, S. Dieckhöfer, T. Quast, S. Seisel, J. Masa, C. Andronesco and W. Schuhmann, *Angew. Chem., Int. Ed.*, 2021, **60**, 9135–9141.
- 61 Z. Zhang, S. Li, Y. Rao, L. Yang, W. Yan and H. Xu, *Chem. Eng. J.*, 2024, **479**, 147376.
- 62 M. Li, S. Kuang, Y. Jin, H. Chi, S. Zhang and X. Ma, *Chem. Eng. J.*, 2025, **506**, 160048.





- 63 M.-G. Kim, J. Park, Y. Choi, H. C. Song, S.-H. Kim, K.-M. Bang, H. C. Ham, N.-K. Kim, D. H. Won, B. K. Min, S. J. Yoo and W. Kim, *Adv. Energy Mater.*, 2023, **13**, 2300749.
- 64 R. Zhang, H. Ma, S. Han, Z. Wu, X. Zhou, Z. Chen, J. Liu, Y. Xiao, W. Chen and K. P. Loh, *Angew. Chem., Int. Ed.*, 2025, **64**, e202421860.
- 65 Z. Ren, B. Li, Y. Wu, H. Liu, F. Guo, S. Tian and J. Yang, *Chem. Eng. J.*, 2025, **507**, 160394.
- 66 L. Yan, W. Su, X. Cao, P. Zhang and Y. Fan, *Chem. Eng. J.*, 2021, **412**, 128718.
- 67 L. Xue, Q.-Y. Fan, Y. Zhao, Y. Liu, H. Zhang, M. Sun, Y. Wang and S. Zeng, *J. Energy Chem.*, 2023, **82**, 414–422.
- 68 S. You, J. Xiao, S. Liang, W. Xie, T. Zhang, M. Li, Z. Zhong, Q. Wang and H. He, *Energy Environ. Sci.*, 2024, **17**, 5795–5818.
- 69 X. Shi, L. Shi, J. Wang, Y. Zhou and S. Zhao, *Matter*, 2024, **7**, 4233–4259.
- 70 F. Huang, X. Chen, H. Sun, Q. Zeng, J. Ma, D. Wei, J. Zhu, Z. Chen, T. Liang, X. Yin, X. Liu, J. Xu and H. He, *Angew. Chem., Int. Ed.*, 2025, **64**, e202415642.
- 71 W. Guo, S. Liu, X. Tan, R. Wu, X. Yan, C. Chen, Q. Zhu, L. Zheng, J. Ma, J. Zhang, Y. Huang, X. Sun and B. Han, *Angew. Chem., Int. Ed.*, 2021, **60**, 21979–21987.
- 72 K. Wang, D. Liu, L. Liu, J. Liu, X. Hu, P. Li, M. Li, A. S. Vasenko, C. Xiao and S. Ding, *eScience*, 2022, **2**, 518–528.
- 73 C. Peng, X. Zhu, Z. Xu, S. Yan, L. Y. Chang, Z. Wang, J. Zhang, M. Chen, T.-K. Sham, Y. Li and G. Zheng, *Small*, 2022, **18**, 2106433.
- 74 C. Li, H. Yan, H. Yang, W. Zhou, C. Xie, B. Pan and Q. Zhang, *Sci. China Mater.*, 2025, **68**, 21–38.
- 75 L. Zhang, J. Feng, S. Liu, X. Tan, L. Wu, S. Jia, L. Xu, X. Ma, X. Song, J. Ma, X. Sun and B. Han, *Adv. Mater.*, 2023, **35**, 2209590.
- 76 X. Zhang, C. Liu, Y. Zhao, L. Li, Y. Chen, F. Raziq, L. Qiao, S.-X. Guo, C. Wang, G. G. Wallace, A. M. Bond and J. Zhang, *Appl. Catal. B Environ. Energy*, 2021, **291**, 120030.
- 77 X. K. Lu, B. Lu, H. Li, K. Lim and L. C. Seitz, *ACS Catal.*, 2022, **12**, 6663–6671.
- 78 H. Zhang, Y. Cao, M. Sun, Y. Liu, Y. Wang, H. Li, R. Zhang, X. Gu and S. Zeng, *Chem. Eng. J.*, 2024, **490**, 151706.
- 79 K. Huang, R. Li, H. Qi, S. Yang, S. An, C. Lian, Q. Xu, H. Liu and J. Hu, *ACS Catal.*, 2024, **14**, 8889–8898.
- 80 H. Wu, J. Li, K. Qi, Y. Zhang, E. Petit, W. Wang, V. Flaud, N. Onofrio, B. Rebiere, L. Huang, C. Salameh, L. Lajaunie, P. Miele and D. Voiry, *Nat. Commun.*, 2021, **12**, 7210.
- 81 A. Bohan, X. Jin, M. Wang, X. Ma, Y. Wang and L. Zhang, *J. Colloid Interface Sci.*, 2024, **654**, 830–839.
- 82 Y. Zhu, J. Sokolowski, X. Song, Y. He, Y. Mei and G. Wu, *Adv. Energy Mater.*, 2020, **10**, 1902844.
- 83 N. Sakamoto, K. Sekizawa, S. Shirai, T. Nonaka, T. Arai, S. Sato and T. Morikawa, *Nat. Catal.*, 2024, **7**, 574–584.
- 84 Z. Sun, C. Li, Z. Wei, F. Zhang, Z. Deng, K. Zhou, Y. Wang, J. Guo, J. Yang, Z. Xiang, P. Ma, H. Zhai, S. Li and W. Chen, *Adv. Mater.*, 2024, **36**, 2404665.
- 85 X.-Q. Wang, Q. Chen, Y.-J. Zhou, H.-M. Li, J.-W. Fu and M. Liu, *Adv. Sens. Energy Mater.*, 2022, **1**, 100023.
- 86 Y. Jia, F. Li, K. Fan and L. Sun, *Adv. Powder Mater.*, 2022, **1**, 100012.
- 87 Y. Chen, Z. Fan, J. Wang, C. Ling, W. Niu, Z. Huang, G. Liu, B. Chen, Z. Lai, X. Liu, B. Li, Y. Zong, L. Gu, J. Wang, X. Wang and H. Zhang, *J. Am. Chem. Soc.*, 2020, **142**, 12760–12766.
- 88 H. Zhang, C. He, S. Han, Z. Du, L. Wang, Q. Yun, W. Cao, B. Zhang, Y.-H. Tian and Q. Lu, *Chin. Chem. Lett.*, 2022, **33**, 3641–3649.
- 89 D. Ma, C. Zhi, Y. Zhang, J. Chen, Y. Zhang and J.-W. Shi, *ACS Nano*, 2024, **18**, 21714–21746.
- 90 Y. Ma, J. Yu, M. Sun, B. Chen, X. Zhou, C. Ye, Z. Guan, W. Guo, G. Wang, S. Lu, D. Xia, Y. Wang, Z. He, L. Zheng, Q. Yun, L. Wang, J. Zhou, P. Lu, J. Yin, Y. Zhao, Z. Luo, L. Zhai, L. Liao, Z. Zhu, R. Ye, Y. Chen, Y. Lu, S. Xi, B. Huang, C.-S. Lee and Z. Fan, *Adv. Mater.*, 2022, **34**, 2110607.
- 91 C. Peng, J. Ma, G. Luo, S. Yan, J. Zhang, Y. Chen, N. Chen, Z. Wang, W. Wei, T.-K. Sham, Y. Zheng, M. Kuang and G. Zheng, *Angew. Chem., Int. Ed.*, 2024, **63**, e202316907.
- 92 L. Li, Y. Zhang, X. Luo, I. Masood ul Hasan, K. Wu, B. Nan, Y. Zhang, N. Xu and J. Qiao, *J. Energy Chem.*, 2023, **86**, 569–578.
- 93 Y. Li, Y. Jin, X. Zong, X. Zhang, G. Li and Y. Xiong, *J. Mater. Chem. A*, 2023, **11**, 11445–11453.
- 94 K. H. Dinh, L. T. Menisa, H. Warkentin, T. N. Nguyen and C.-T. Dinh, *ACS Catal.*, 2025, **15**, 5731–5759.
- 95 Q. Tang, Q. Hao, Q. Zhu, J. Wu, K. Huang, K. Liu and J. Lu, *Adv. Energy Mater.*, 2025, **15**, 2403778.
- 96 J. Chen, M. R. Ahasan, J.-S. Oh, J. A. Tan, S. Hennessey, M. M. Kaid, H. M. El-Kaderi, L. Zhou, K. U. Lao, R. Wang and W.-N. Wang, *J. Mater. Chem. A*, 2024, **12**, 4601–4609.
- 97 M. Wu, F. Dong, Y. Yang, X. Cui, X. Liu, Y. Zhu, D. Li, S. Omanovic, S. Sun and G. Zhang, *Electrochem. Energy Rev.*, 2024, **7**, 10.
- 98 J. Hu, M. Zhou, K. Li, A. Yao, Y. Wang, Q. Zhu, Y. Zhou, L. Huang, Y. Pei, Y. Du, S. Jin and M. Zhu, *Small*, 2023, **19**, 2301357.
- 99 L. Huang, Z. Liu, G. Gao, C. Chen, Y. Xue, J. Zhao, Q. Lei, M. Jin, C. Zhu, Y. Han, J. S. Francisco and X. Lu, *J. Am. Chem. Soc.*, 2023, **145**, 26444–26451.
- 100 Z. Zhang, G. Wen, D. Luo, B. Ren, Y. Zhu, R. Gao, H. Dou, G. Sun, M. Feng, Z. Bai, A. Yu and Z. Chen, *J. Am. Chem. Soc.*, 2021, **143**, 6855–6864.
- 101 Y. Lu, H. Li, H. Sun, J. Zhao, Y. Zhang, Y. Wang, C. Zhu, D. Gao, Y. Tuo, J. Zeng, D. Chen and Z. Yan, *ACS Catal.*, 2024, **14**, 14744–14753.
- 102 H. Yu, W. Zhao, X. Dong, J. Wang, W. Wang, L.-L. Shen, G.-R. Zhang and D. Mei, *Appl. Catal. B Environ. Energy*, 2025, **363**, 124805.
- 103 Y. Hu, D. Lu, W. Zhou, X. Wang and Y. Li, *J. Mater. Chem. A*, 2023, **11**, 1937–1943.
- 104 S. Yan, Z. Chen, Y. Chen, C. Peng, X. Ma, X. Lv, Z. Qiu, Y. Yang, Y. Yang, M. Kuang, X. Xu and G. Zheng, *J. Am. Chem. Soc.*, 2023, **145**, 26374–26382.
- 105 W. Zhu, L. Zhang, P. Yang, X. Chang, H. Dong, A. Li, C. Hu, Z. Huang, Z.-J. Zhao and J. Gong, *Small*, 2018, **14**, 1703314.



- 106 X. Yao, D. Cui, C. Zhu, J. He, F. Meng, S. Yang, M. Dong, G. Shan, M. Zhang, C. Sun, X. Wang and Z. Su, *ACS Mater. Lett.*, 2024, **6**, 5112–5119.
- 107 H. Wang, G. Zhan, C. Tang, D. Yang, W. Liu, D. Wang, Y. Wu, H. Wang, K. Liu, J. Li, M. Huang and K. Chen, *ACS Nano*, 2023, **17**, 4790–4799.
- 108 R. Nankya, Y. Xu, A. Elgazzar, P. Zhu, T.-U. Wi, C. Qiu, Y. Feng, F. Che and H. Wang, *Angew. Chem., Int. Ed.*, 2024, **63**, e202403671.
- 109 Q. Zhang, J. Peng, S. Jiang, H. Xiong, X. Fu, S. Shang, J. Xu, G. He and P.-C. Chen, *Appl. Catal. B Environ. Energy*, 2025, **371**, 125255.
- 110 Z. Zhang, Q. Fang, X. Yang, S. Zuo, T. Cheng, Y. Yamauchi and J. Tang, *Adv. Mater.*, 2025, **37**, 2411498.
- 111 Z. Niu, X. Gao, S. Lou, N. Wen, J. Zhao, Z. Zhang, Z. Ding, R. Yuan, W. Dai and J. Long, *ACS Catal.*, 2023, **13**, 2998–3006.
- 112 R. Belgamwar, R. Verma, T. Das, S. Chakraborty, P. Sarawade and V. Polshettiwar, *J. Am. Chem. Soc.*, 2023, **145**, 8634–8646.
- 113 R. Chen, J. Zhao, X. Zhang, Q. Zhao, Y. Li, Y. Cui, M. Zhong, J. Wang, X. Li, Y. Huang and B. Liu, *J. Am. Chem. Soc.*, 2024, **146**, 24368–24376.
- 114 M. Qi, Y. Ma, C. Zhang, B. Li, X. Yang, Z. Shi, S. Liu, C. An, J. Jiao and T. Lu, *Sci. China Chem.*, 2025, **68**, 1620–1626.
- 115 E. Landaeta, N. I. Kadosh and Z. D. Schultz, *ACS Catal.*, 2023, **13**, 1638–1648.
- 116 Y. Hu, D. Lu, W. Zhou, X. Wang and Y. Li, *J. Mater. Chem. A*, 2023, **11**, 1937–1943.
- 117 X. Dong, S. Li, C. Zhu, J. Mao, G. Wu, G. Li, G. Feng, A. Chen, Y. Wei, X. Liu, J. Wang, Y. Song, W. Chen and W. Wei, *Appl. Catal. B Environ. Energy*, 2023, **336**, 122929.
- 118 H. Liu, C. Yang, T. Bian, H. Yu, Y. Zhou, Y. Zhang and L. Sun, *Adv. Energy Mater.*, 2025, 2405658.
- 119 Y. Shao, Q. Yuan and J. Zhou, *Small*, 2023, **19**, 2303446.
- 120 J. Zhao and S. Lin, *J. Colloid Interface Sci.*, 2025, **680**, 257–264.
- 121 H. Liu, C. Yang, T. Bian, H. Yu, Y. Zhou and Y. Zhang, *Angew. Chem., Int. Ed.*, 2024, **63**, e202404123.
- 122 Q. Hao, H.-x. Zhong, J.-z. Wang, K.-h. Liu, J.-m. Yan, Z.-h. Ren, N. Zhou, X. Zhao, H. Zhang, D.-x. Liu, X. Liu, L.-w. Chen, J. Luo and X.-b. Zhang, *Nat. Synth.*, 2022, **1**, 719–728.
- 123 X. Zhao, K. Zhao, Y. Liu, Y. Su, S. Chen, H. Yu and X. Quan, *ACS Catal.*, 2022, **12**, 11412.
- 124 L.-M. Cao, H.-H. Huang, J.-W. Wang, D.-C. Zhong and T.-B. Lu, *Green Chem.*, 2018, **20**, 798–803.
- 125 Y.-N. Gong, C.-Y. Cao, W.-J. Shi, J.-H. Zhang, J.-H. Deng, T.-B. Lu and D.-C. Zhong, *Angew. Chem., Int. Ed.*, 2022, **61**, e202215187.
- 126 X.-M. Liang, H.-J. Wang, C. Zhang, D.-C. Zhong and T.-B. Lu, *Appl. Catal. B Environ. Energy*, 2023, **322**, 122073.
- 127 Z.-W. Chen, H.-J. Wang, C. Liu, X.-L. Lu and T.-B. Lu, *Sci. China Chem.*, 2025, **68**, 570–579.
- 128 Y. Wang, B. J. Park, V. K. Paidi, R. Huang, Y. Lee, K.-J. Noh, K.-S. Lee and J. W. Han, *ACS Energy Lett.*, 2022, **7**, 640–649.
- 129 S. Chen, X. Zheng, P. Zhu, Y. Li, Z. Zhuang, H. Wu, J. Zhu, C. Xiao, M. Chen, P. Wang, D. Wang and Y.-L. He, *Angew. Chem., Int. Ed.*, 2024, **63**, e202411591.
- 130 G. Yasin, A. Kumar, S. Ajmal, M. Asim Mushtaq, M. Tabish, A. Saad, M. A. Assiri, M. Tariq Nazir and Q. Zhuo, *Coord. Chem. Rev.*, 2024, **501**, 215589.
- 131 L. Zhang, J. Feng, L. Wu, X. Ma, X. Song, S. Jia, X. Tan, X. Jin, Q. Zhu, X. Kang, J. Ma, Q. Qian, L. Zheng, X. Sun and B. Han, *J. Am. Chem. Soc.*, 2023, **145**, 21945–21954.
- 132 J.-d. Yi, X. Gao, H. Zhou, W. Chen and Y. Wu, *Angew. Chem., Int. Ed.*, 2022, **61**, e202212329.
- 133 Z. Guo, H. Zhu, G. Yang, A. Wu, Q. Chen, Z. Yan, K. Loon Fow, H. Do, J. D. Hirst, T. Wu and M. Xu, *Chem. Eng. J.*, 2023, **476**, 146556.
- 134 W. Xie, H. Li, G. Cui, J. Li, Y. Song, S. Li, X. Zhang, J. Y. Lee, M. Shao and M. Wei, *Angew. Chem., Int. Ed.*, 2021, **60**, 7382–7388.
- 135 H. Zhang, X. Wang, Y. Sun, X. Wang, Z. Tang, S. Li, X. Gao, J. Wang, Z. Hou, K. Nie, J. Xie, Z. Yang and Y.-M. Yan, *Appl. Catal. B Environ. Energy*, 2024, **351**, 123992.
- 136 T. Zhang, B. Yuan, W. Wang, J. He and X. Xiang, *Angew. Chem., Int. Ed.*, 2023, **62**, e202302096.
- 137 L. Yin, Z. Li, J. Feng, P. Zhou, L. Qiao, D. Liu, Z. Yi, W. F. Ip, G. Luo and H. Pan, *ACS Appl. Mater. Interfaces*, 2023, **15**, 47135–47144.
- 138 M. Wang, H. Chen, M. Wang, J. Wang, Y. Tuo, W. Li, S. Zhou, L. Kong, G. Liu, L. Jiang and G. Wang, *Angew. Chem., Int. Ed.*, 2023, **62**, e202306456.
- 139 Y. Cao, S. Chen, S. Bo, W. Fan, J. Li, C. Jia, Z. Zhou, Q. Liu, L. Zheng and F. Zhang, *Angew. Chem., Int. Ed.*, 2023, **62**, e202303048.
- 140 L. Chen, J. Chen, W. Fu, J. Chen, D. Wang, Y. Xiao, S. Xi, Y. Ji and L. Wang, *Nat. Commun.*, 2024, **15**, 7053.
- 141 A. Saxena, S. Kapila, J. E. Medvedeva and M. Nath, *ACS Appl. Mater. Interfaces*, 2023, **15**, 14433–14446.
- 142 F. Chang, K. Zhu, C. Liu, J. Wei, S. Yang, Q. Zhang, L. Yang, X. Wang and Z. Bai, *Adv. Funct. Mater.*, 2024, **34**, 2400893.
- 143 R. Yun, F. Zhan, X. Wang, B. Zhang, T. Sheng, Z. Xin, J. Mao, S. Liu and B. Zheng, *Small*, 2021, **17**, 2006951.
- 144 Y. Jiang, C. Lv, B. Lu, Y. Song, T. Liu, X. Zhang, D. Gao, K. Ye and G. Wang, *ACS Nano*, 2025, **19**, 11263–11272.
- 145 S. Shen, X. Peng, L. Song, Y. Qiu, C. Li, L. Zhuo, J. He, J. Ren, X. Liu and J. Luo, *Small*, 2019, **15**, 1902229.
- 146 P. Luan, X. Dong, L. Liu, J. Xiao, P. Zhang, J. Zhang, H. Chi, Q. Wang, C. Ding, R. Li and C. Li, *ACS Catal.*, 2024, **14**, 8776–8785.
- 147 M. Chhetri, M. Wan, Z. Jin, J. Yeager, C. Sandor, C. Rapp, H. Wang, S. Lee, C. J. Bodenschatz, M. J. Zachman, F. Che and M. Yang, *Nat. Commun.*, 2023, **14**, 3075.
- 148 Y. Zheng, J. Zhang, Z. Ma, G. Zhang, H. Zhang, X. Fu, Y. Ma, F. Liu, M. Liu and H. Huang, *Small*, 2022, **18**, 2201695.
- 149 X. Li, M. Qin, X. Wu, X. Lv, J. Wang, Y. Wang and H. B. Wu, *Small*, 2023, **19**, 2302530.
- 150 Z. Wei, S. Yue, S. Gao, M. Cao and R. Cao, *Nano Res.*, 2023, **16**, 7777–7783.
- 151 T. Wan, C. Lv, K. Ye, M. Ma, D. Hu, J. Xiao and W. Xiao, *Small Methods*, 2025, 2500005.



- 152 X. Liu, T. Liu, T. Ouyang, J. Deng and Z.-Q. Liu, *Angew. Chem., Int. Ed.*, 2025, **64**, e202419796.
- 153 H. Zhang, X. Wang, Y. Sun, X. Wang, Z. Tang, S. Li, X. Gao, J. Wang, Z. Hou, K. Nie, J. Xie, Z. Yang and Y.-M. Yan, *Appl. Catal. B Environ. Energy*, 2024, **351**, 123992.
- 154 Y. Xiao, F. Yu, C. Xia, D. Zhu, J. Chen, N. Liu, Y. Zhao, R. Qi, W. Guo, B. You, T. Yao, Y. Pang, Z. Wang, H. Wang, F. Song and B. Y. Xia, *J. Am. Chem. Soc.*, 2025, **147**, 15654–15665.
- 155 Z. Guo, H. Zhu, Z. Yan, L. Lei, D. Wang, Z. Xi, Y. Lian, J. Yu, K. L. Fow, H. Do, J. D. Hirst, T. Wu and M. Xu, *Appl. Catal. B Environ. Energy*, 2025, **364**, 124839.
- 156 Z. Yang, D. Ji, Z. Li, Z. He, Y. Hu, J. Yin, Y. Hou, P. Xi and C.-H. Yan, *Small*, 2023, **19**, 2303099.
- 157 J. Feng, L. Wu, S. Liu, L. Xu, X. Song, L. Zhang, Q. Zhu, X. Kang, X. Sun and B. Han, *J. Am. Chem. Soc.*, 2023, **145**, 9857–9866.
- 158 H. Wang, H. Zhang, Y. Huang, H. Wang, A. Ozden, K. Yao, H. Li, Q. Guo, Y. Liu, A. Vomiero, Y. Wang, Z. Qian, J. Li, Z. Wang, X. Sun and H. Liang, *ACS Nano*, 2023, **17**, 346–354.
- 159 J. Liu, P. Li, S. Jia, Y. Wang, L. Jing, Z. Liu, J. Zhang, Q. Qian, X. Kang, X. Sun, Q. Zhu and B. Han, *Nat. Synth.*, 2025, DOI: [10.1038/s44160-025-00752-4](https://doi.org/10.1038/s44160-025-00752-4).
- 160 J. Feng, L. Wu, X. Song, L. Zhang, S. Jia, X. Ma, X. Tan, X. Kang, Q. Zhu, X. Sun and B. Han, *Nat. Commun.*, 2024, **15**, 4821.
- 161 X. Zhou, J. Shan, L. Chen, B. Y. Xia, T. Ling, J. Duan, Y. Jiao, Y. Zheng and S. Qiao, *J. Am. Chem. Soc.*, 2022, **144**, 2079–2084.

